nature

https://doi.org/10.1038/s41586-021-03562-8

Accelerated Article Preview

PIK3CA and CCM mutations fuel cavernomas through a cancer-like mechanism

Received: 25 August 2020

Accepted: 16 April 2021

Accelerated Article Preview Published online 28 April 2021

Cite this article as: Ren, A. A. et al. *PIK3CA* and CCM mutations fuel cavernomas through a cancer-like mechanism. *Nature* https://doi.org/10.1038/s41586-021-03562-8 (2021).

Aileen A. Ren, Daniel A. Snellings, Yourong S. Su, Courtney C. Hong, Marco Castro, Alan T. Tang, Matthew R. Detter, Nicholas Hobson, Romuald Girard, Sharbel Romanos, Rhonda Lightle, Thomas Moore, Robert Shenkar, Christian Benavides, M. Makenzie Beaman, Helge Mueller-Fielitz, Mei Chen, Patricia Mericko, Jisheng Yang, Derek C. Sung, Michael T. Lawton, Michael Ruppert, Markus Schwaninger, Jakob Körbelin, Michael Potente, Issam A. Awad, Douglas A. Marchuk & Mark L. Kahn

Article

PIK3CA and CCM mutations fuel cavernomas through a cancer-like mechanism

https://doi.org/10.1038/s41586-021-03562-8

Received: 25 August 2020

Accepted: 16 April 2021

Published online: 28 April 2021

Aileen A. Ren[1,12], Daniel A. Snellings[2,12], Yourong S. Su[3], Courtney C. Hong[1], Marco Castro[4], Alan T. Tang[1], Matthew R. Detter[2], Nicholas Hobson[5], Romuald Girard[5], Sharbel Romanos[5], Rhonda Lightle[5], Thomas Moore[5], Robert Shenkar[5], Christian Benavides[2], M. Makenzie Beaman[2], Helge Mueller-Fielitz[8], Mei Chen[1], Patricia Mericko[1], Jisheng Yang[1], Derek C. Sung[1], Michael T. Lawton[6], Michael Ruppert[7], Markus Schwaninger[8], Jakob Körbelin[9], Michael Potente[4,10,11], Issam A. Awad[5], Douglas A. Marchuk[2]✉ & Mark L. Kahn[1]✉

Vascular malformations are considered monogenic disorders that result in dysregulated vessel growth. Cerebral cavernous malformations (CCMs) arise owing to inactivation of the endothelial CCM protein complex required to dampen MEKK3 activity[1–4]. Environmental factors explain differences in CCM natural history between individuals[5], but why single CCMs often exhibit sudden, rapid growth culminating in stroke or seizure is unknown. Here we demonstrate that CCM growth requires increased PI3K-mTOR signalling and loss of CCM function. We identify *PIK3CA* gain of function (GOF) and CCM loss of function (LOF) somatic mutations in the same cells in a majority of human CCMs. Using mouse models, we show that CCM growth requires both PI3K GOF and CCM LOF in endothelial cells, and that both CCM LOF and increased expression of the transcription factor KLF4, a downstream MEKK3 effector, augment mTOR signalling in endothelial cells. Consistent with these findings, the mTORC1 inhibitor Rapamycin effectively blocks CCM formation in mouse models. We establish a three-hit mechanism analogous to cancer in which aggressive vascular malformations arise through the loss of vascular "suppressor genes" that constrain vessel growth and gain of a vascular "oncogene" that stimulates excess vessel growth. These findings suggest that aggressive CCMs may be treated using clinically approved mTORC1 inhibitors.

Vascular malformations such as cerebral cavernous malformations (CCMs) that arise in the central nervous system are an important cause of stroke and disability in younger individuals[6]. Classic genetic studies have supported a monogenic basis for CCM disease associated with biallelic loss of function (LOF) mutations in three genes, *KRIT1, CCM2*, and *PDCD10*, that encode the components of a heterotrimeric CCM protein complex[7,8]. Mouse models have further revealed that deletion of any of the CCM genes in brain endothelial cells of neonatal mice confers CCM lesions due in part to increased MEKK3-KLF2/4 signaling[1–4].

Serial imaging of human CCMs has revealed that most are slow-growing and clinically silent[9]. In contrast, those that cause stroke and seizure are typically fast-growing and associated with repeated lesional hemorrhage[10,11]. Such aggressive, symptomatic lesions are surgically resected if possible to prevent or treat associated neurologic complications, but surgery is associated with high morbidity and cost and is impractical for patients with multiple lesions or lesions in less surgically-accessible locations. Why a subset of CCM lesions exhibits rapid growth associated with clinical symptoms is unknown. The studies described below reveal that symptomatic CCM disease arises through a cancer-like paradigm in which the accumulation of multiple somatic mutations in the same cell results in both the loss of a vascular malformation suppressor gene (i.e. the CCM gene) and the gain of vascular malformation growth gene (i.e. *PIK3CA*).

Mature mice form testicular cavernomas

CCMs arise in the angiogenic vascular beds of the neonatal retina and hindbrain following genetic endothelial cell deletion of *Krit1*, *Ccm2* or *Pdcd10* in mice[2,12–15]. Unlike human CCM lesions, however, CCMs do not form following endothelial gene deletion in adult mice

[1]Department of Medicine and Cardiovascular Institute, University of Pennsylvania, Philadelphia, PA, USA. [2]Department of Molecular Genetics and Microbiology, Duke University School of Medicine, Durham, NC, USA. [3]Department of Neurosurgery, University of Pennsylvania, Philadelphia, PA, USA. [4]Angiogenesis and Metabolism Laboratory, Max Planck institute for Heart and Lung Research, Bad Nauheim, Germany. [5]Neurovascular Surgery Program, Section of Neurosurgery, Department of Surgery, The University of Chicago Medicine and Biological Sciences, Chicago, IL, USA. [6]Department of Neurosurgery, The Barrow Neurological Institute, Phoenix, AZ, USA. [7]Cancer Institute, West Virginia University, Morgantown, WV, USA. [8]Institute for Experimental and Clinical Pharmacology and Toxicology, Center of Brain, Behavior and Metabolism, University of Lubeck, Lubeck, Germany. [9]University Medical Center Hamburg-Eppendorf, Department of Oncology, Hematology and Bone Marrow Transplantation, Hamburg, Germany. [10]Berlin Institute of Health (BIH) and Charité – Universitätsmedizin Berlin, corporate member of Freie Universität Berlin, Humboldt-Universität zu Berlin, Berlin, Germany. [11]Max Delbrück Center for Molecular Medicine (MDC), Berlin, Germany. [12]These authors contributed equally: Aileen A. Ren, Daniel A. Snellings. ✉e-mail: douglas.marchuk@duke.edu; markkahn@pennmedicine.upenn.edu

(Extended Data Fig. 1a-d and[2,12,14]). We administered tamoxifen to 2-month-old *Cdh5*-CreERT2;*Krit1*$^{fl/fl}$ ("*Krit1*^{iECKO}") animals, and examined all organs at 6 months. The vasculature of all organs appeared unchanged with the exception of the testis that appeared bloody and swollen (Extended Data Fig. 1e). Histologic examination revealed testicular cavernomas like those in the brain (Extended Data Fig. 1e vs. 1b and[2,16]). Molecular hallmarks of brain CCM include elevated expression of the KLF4 transcription factor and peri-vascular staining for DPEAAE, a marker of ADAMTS-cleaved versican[1,2,17,18], both of which were detected in testicular cavernomas (Extended Data Fig. 1f-h). Although no CCMs formed in the brain, immunostaining revealed elevated KLF4 levels in the brain endothelial cells of adult *Krit1*^{iECKO} animals (Extended Data Fig. 1f). Thus endothelial loss of KRIT1 in mature mice is sufficient to confer cavernous vascular malformations in the testis, but not in the brain, despite increased downstream MEKK3-KLF2/4 signaling at both sites.

PIK3CA GOF synergizes with CCM LOF in mice

Since testicular endothelial cells exhibit the highest rate of basal proliferation of those in all organs[19], we hypothesized that CCM formation might require proliferative signals. GOF mutations in phosphatidylinositol-4,5-bisphosphate 3-kinase catalytic subunit alpha (PIK3CA) drive cell proliferation in cancer and confer venous and lymphatic malformations when they arise in endothelial cells[20–25]. To test whether genetic gain of PIK3CA function might augment CCM formation in vivo we used the *Slco1c1*(BAC)-CreERT2 transgene to drive expression of PIK3CA H1047R (using a R26-LSL-*Pik3ca*^{H1047R} allele, "i*Pik3ca*^{H1047R}") exclusively in brain endothelial cells[5,26]. To stringently test for interaction with CCM LOF, we used a *Krit1*$^{fl/fl}$ colony that fails to develop CCM lesions in neonatal mice following loss of KRIT1 alone due to the presence of a "resistant" gut microbiome that reduces basal MEKK3-KLF2/4 signaling[5]. Following tamoxifen administration at P1, we examined *Slco1c1*(BAC)-CreERT2;*Krit*$^{fl/fl}$ ("*Krit1*^{iBECKO}"), *Slco1c1*(BAC)-CreERT2;i*Pik3ca*^{H1047R} ("*Pik3ca*^{iBECGOF}"), and *Krit1*^{iBECKO};*Pik3ca*^{iBECGOF} littermates at P7 (Fig. 1a). *Krit1*^{iBECKO} animals with a resistant microbiome failed to develop CCM lesions (Fig. 1b, c), while *Pik3ca*^{iBECGOF} animals developed small vascular lesions in both the hindbrain and forebrain (Fig. 1b, c). Visual and microCT analysis revealed a synergistic effect of CCM LOF and PIK3CA GOF on lesion formation in *Krit1*^{iBECKO};*Pik3ca*^{iBECGOF} double mutants (Fig. 1b, c). Hematoxylin-eosin staining of hindbrain sections revealed dilated, blood-filled post-capillary venules and veins in the white matter of P6 *Pik3ca*^{iBECGOF} animals, the site where CCM lesions also first arise (Extended Data Fig. 2 and[2]). Endothelial loss of PTEN, a well-characterized inhibitor of PI3K signaling, similarly augmented CCM formation in a dose-dependent manner in neonatal animals (Extended Data Fig. 3).

The findings described above suggested that, in addition to CCM LOF, CCM formation might require a threshold level of endothelial PI3K activity that is lacking in the adult brain. To test this hypothesis we first attempted to induce PIK3CA GOF and CCM LOF in the brain endothelial cells of adult mice using the *Slco1c1*(BAC)-CreERT2 transgene. However, lethal spontaneous neurologic symptoms associated with large single lesions were observed in *Slco1c1*(BAC)-CreERT2;*Krit1*$^{fl/fl}$;i*Pik3ca*^{H1047R} animals, but not single mutant littermates, in the absence of tamoxifen administration (Extended Data Fig. 4a-e). Cre reporter expression revealed leaky Cre activity that was 99% restricted to the vascular endothelial cell population (Extended Data Fig. 4f, g). These studies revealed that Cre-mediated recombination is sufficient for lesion formation in older animals only if it results in both PIK3CA GOF and CCM LOF, and that this synergy is mediated by interaction within or between endothelial cells.

To more rigorously test synergy in adult animals we next created cranial windows through which to directly inject viral AAV vector encoding Cre recombinase into the brains of *Krit1*$^{fl/fl}$, *Krit1*$^{fl/+}$;i*Pik3ca*^{H1047R}, and *Krit1*$^{fl/fl}$;i*Pik3ca*^{H1047R} littermates at age 2 months (Fig. 1d-g and Extended Data Fig. 5a-c). Cre reporter expression revealed Cre activity in both endothelial and neuronal cells following direct injection (Extended Data Fig. 6). AAV-Cre injection into *Krit1*$^{fl/fl}$ or *Krit1*$^{fl/+}$;i*Pik3ca*^{H1047R} animals failed to induce lesion formation at 21 days. In contrast, injection into *Krit1*$^{fl/fl}$;i*Pik3ca*^{H1047R} animals resulted in the formation of large cavernomas at the site of injection that exhibited a classic "mulberry-like" appearance and peri-lesional iron deposition characteristic of human CCMs[27] (Fig. 1e–g and Extended Data Fig. 5b-d). These studies demonstrate that neither CCM LOF nor PIK3CA GOF alone is sufficient for lesion formation in the mature brain, but that the combination of the two results in the rapid formation of CCM lesions.

PIK3CA and CCM mutations in human CCMs

To determine whether human CCM lesions harbor mutations in *PIK3CA* or other cell proliferation genes, we sequenced 79 surgically resected CCM lesions on a panel of 66 genes including the CCM genes and *PIK3CA*. Lesions were classified as "familial", "sporadic" or "unknown" based on genetic and clinical evidence. 68 surgically resected human brain arteriovenous malformations (bAVMs) served as a control set to determine if somatic mutations identified were unique to CCMs. We identified GOF *PIK3CA* somatic mutations in 56/79 (71%) CCMs and 0/68 bAVMs (Fig. 2a, b and Supplementary Table 1). Mutations in *PIK3CA* were present in both familial (14/21) and sporadic (12/15) CCMs (Fig. 2a, b) at <20% allele frequency (Extended Data Fig. 7a). All *PIK3CA* mutations occurred at known hotspots in the catalogue of somatic mutations in cancer (COSMIC), and activate PI3K signaling[28] (Fig. 2c).

Consistent with prior studies[29–31], somatic mutations in CCM genes were identified in 24/79 (30%) of CCM lesions. Three distinct genetic hits (two CCM alleles and one *PIK3CA* allele) were detected in 9 samples of familial CCM (‡ on Fig. 2a) and 6 samples of presumed sporadic CCM (* on Fig. 2a), indicating that no fewer than three independent somatic mutation events occurred in these lesions.

To determine whether the *PIK3CA* and CCM gene somatic mutations arise in the same cell in human CCMs, we next performed single-nucleus DNA sequencing (snDNA-seq) on 3 sporadic and 2 familial CCMs. Nuclei isolated from frozen tissue were sorted, and partitioned into microfluidic droplets from which the *KRIT1, CCM2, PDCD10*, and *PIK3CA* exons were amplified (Fig. 2d and Extended Data Fig. 7b-e). snDNA-seq of sporadic CCMs (5003, 5038, and 5079) and familial CCMs (5065 and 5073) revealed that the majority of mutant nuclei harbored all identified CCM and *PIK3CA* somatic mutations (Fig. 2e and Extended Data Fig. 7f). A smaller number of nuclei showed each of the possible genotype combinations (Extended Data Fig. 7f), consistent with allelic dropout (ADO), a common technical artifact in single-nucleus/cell DNA sequencing data[32]. By comparing the ratio of heterozygous to homozygous nuclei for informative SNPs in our samples, we estimate the rate of ADO to be 8.4% ± 4.1%. Despite this confounder, snDNA-seq reveals that *PIK3CA* and CCM gene somatic mutations arise in the same cell in human CCMs.

CCM LOF and PIK3CA GOF activate mTOR

A primary mechanism by which loss of CCM function promotes lesion formation is through gain of MEKK3 activity and increased expression of the KLF2 and KLF4 transcription factors in endothelial cells[1,2,17,33]. Since either CCM LOF or PIK3CA GOF alone is sufficient to drive formation of dilated venous vessels of the white matter (Extended Data Fig. 2), we first addressed whether PIK3CA GOF might also induce an increase in KLF2 and KLF4 expression in neonatal brain endothelial cells (Extended Data Fig. 8a). Consistent with prior studies, immunostaining of lesional endothelium and qPCR analysis of brain endothelial cells isolated from P6 *Krit1*^{BECKO} animals with a susceptible gut microbiome exhibited high KLF4 protein and *Klf4* mRNA expression (Extended Data Fig. 8b, c). In contrast, the endothelial cells lining vascular lesions or

isolated from P6 *Pik3ca*^{iBECGOF} hindbrains did not express elevated levels of KLF4 protein or mRNA (Extended Data Fig. 8b, c). Similarly, while knockdown of CCM genes in cultured human umbilical vein endothelial cells (HUVECs) conferred an increase in *KLF2* and *KLF4* gene expression, expression of PIK3CA H1047R did not (Extended Data Fig. 8d and[1,2]). These studies suggest that PI3K signaling is unlikely to act upstream of the MEKK3-KLF2/4 pathway.

We next assessed whether the two pathways might intersect at the level of PI3K and/or mTORC1 signaling. mTORC1 activity results in phosphorylation of ribosomal protein S6 (S6). Consistent with PI3K GOF, neonatal *Pik3ca*^{iBECGOF} brain sections exhibited high phospho-S6 levels in endothelial cells lining venous lesions (Fig. 3a). Strikingly, elevated phospho-S6 levels were also detected in the endothelial cells lining CCM lesions in the white matter of P6 *Krit1*^{BECKO} brains (Fig. 3a). Immunoblotting of cell lysate from P6 *Krit1*^{BECKO} and control brain endothelial cells confirmed elevated S6 phosphorylation at Ser235/236 and Ser240/244 in KRIT1-deficient brain endothelial cells (Fig. 3b, c). siRNA-mediated CCM LOF in HUVECs conferred similar increases in phospho-S6 (Fig. 3d, e). In contrast to phospho-S6, significant changes in phospho-AKT were not detected in P6 *Krit1*^{BECKO} brain endothelial cells or cultured endothelial cells exposed to *KRIT1* siRNA (Fig. 3b–e). These studies reveal that CCM LOF augments mTORC1 activity in endothelial cells both in vivo and ex vivo.

KLF4 augments EC PI3K-mTOR signaling

Prior studies have identified increased brain endothelial expression of KLF4 as a causal downstream effector mechanism of CCM formation in vivo[1,2,17]. To further elucidate the relationship between CCM LOF and PI3K-mTOR signaling, we next induced KLF4 expression in *Slco1c1*(BAC)-Cre; R26-LSL-rtTA;tetO-KLF4 ("KLF4^{iBECGOF}") animals by doxycycline administration starting at P1 (Extended Data Fig. 9a, b). Induction of KLF4 expression resulted in the formation of vascular lesions associated with peri-lesional hemorrhage by P6 (Fig. 3f and Extended Data Fig. 9b, c). Like those conferred by CCM LOF or PIK3CA GOF, lesions in KLF4^{iBECGOF} animals arose primarily in the veins and post-capillary venules of the white matter (Extended Data Fig. 9c). Immunostaining revealed elevated endothelial phospho-S6 in KLF4^{iBECGOF} animals (Fig. 3g and Extended Data Fig. 9d), a finding similar to that observed in *Krit1*^{BECKO} animals (Fig. 3a). Expression of a KLF4-GFP fusion protein in HUVECs using a tetracycline-inducible lentivirus conferred increased levels of the known KLF4 target gene eNOS as well as both phospho-S6 and phospho-AKT (Fig. 3h, i and Extended Data Fig. 9e). Thus increased expression of the causal downstream CCM effector KLF4 is sufficient to confer white matter venous lesions like those conferred by either CCM LOF or PI3K GOF in association with increased PI3K-mTORC1 signaling (Fig. 3j). Importantly, these studies do not exclude PI3K-independent mechanisms by which CCM LOF may also synergize with PI3K GOF.

Rapamycin prevents CCM formation in mice

The findings that PIK3CA GOF supports CCM formation in both adult mice and humans and that both CCM LOF and KLF4 GOF increase endothelial cell phospho-S6 suggested that increased mTOR activity may be required for CCM formation. Rapamycin (aka Sirolimus) is an FDA-approved mTORC1 inhibitor that is an effective therapy for venous and lymphatic malformations that arise due to PIK3CA GOF mutations[20–25] identical to those we identified in human CCM lesions (Fig. 2). We therefore tested the ability of Rapamycin to prevent CCM formation in mice. *Krit1* was constitutively deleted in the brain endothelial cells of neonatal *Krit1*^{BECKO} animals with a susceptible microbiome, a single Rapamycin dose (50 micrograms) administered at P2, and CCM lesions assessed at P10 (Fig. 4a). Single dose rapamycin treatment reduced lesion formation in the neonatal model by approximately 75% compared with vehicle alone (P<0.001, Fig. 4b, c). To test its effect on CCM lesions that arise due to compound CCM LOF mutations and PIK3CA GOF mutations like those identified in resected human lesions, Rapamycin was administered daily at either low dose (100 micrograms) or high dose (400 micrograms) starting 7 days after cranial window surgery and viral Cre injection in the adult model (Fig. 4d), a timepoint that coincides with the earliest visual lesion detection of CCM lesions (Extended Data Fig. 5). Rapamycin treatment virtually ablated CCM growth using either low or high dose treatments (Fig. 4e, f and Extended Data Fig. 10a-d). Consistent with a downstream mechanism of action, Rapamycin treatment ablated the rise in phospho-S6 but not the rise in KLF4 in *Krit1*^{BECKO} brain endothelial cells (Extended Data Fig. 10e-g) and reduced lesion volume by approximately 68% in KLF4^{iBECGOF} animals (Fig. 4g–i). These concordant findings (i) are consistent with a mechanism in which S6 activation is downstream of MEKK3-KLF2/4 signaling (Fig. 3j), (ii) support a central role for mTOR signaling in CCM pathogenesis, and (iii) identify Rapamycin as a potentially powerful and available drug to treat CCM disease.

Discussion

The most significant conceptual advance of this study is the discovery of a compound genetic mechanism of vascular malformation pathogenesis. While vascular malformations have been considered monogenic in origin, our studies identify a digenic, "triple-hit" mechanism involving the acquisition of as many as three distinct genetic mutations that culminate in CCM LOF and *PIK3CA* GOF as the basis for rapidly growing, clinically symptomatic CCMs. By analogy to cancer, the CCM genes may be considered vascular "suppressor genes", required to constrain vessel growth, while *PIK3CA* may be considered a vascular "oncogene", capable of driving excess vascular growth. As in cancer, the combined loss of a vascular suppressor and gain of a vascular activator is a potent combination that culminates in aggressive, symptomatic disease.

A clinical clue to the pathogenesis of human CCM disease that may be explained by our findings is the observation that sporadic CCMs frequently arise at sites of pre-existing developmental venous anomalies (DVAs) (24-32% assessed by MRI, and up to 100% in one surgical assessment[11,34]). DVA is found in a majority of individuals with Cowden syndrome, an inherited disease caused by germline heterozygous LOF mutations in *PTEN* that confer gain of PI3K function[35]. A parsimonious explanation for these observations is that endothelial cells with pre-existing *PIK3CA* mutations sufficient to confer DVA subsequently acquire CCM LOF mutations and transform into more aggressive sporadic CCM lesions. While such a molecular pathogenesis remains entirely speculative until DVA genetic sequencing is performed, it would support a mechanism highly analogous to cancer in which accrued mutations convert a benign vascular abnormality into a more malignant one.

Immediately translatable findings of this study are that PIK3CA GOF plays a causal role in the growth of clinically symptomatic, aggressive CCM lesions, and that mTORC1 inhibition using an approved drug may slow or arrest this growth. Although aggressive CCM lesions are relatively rare, they account for virtually all of the strokes and neurologic symptoms associated with this disease and they can presently only be treated by surgical resection. Sirolimus has recently been used successfully to treat lymphatic and venous/slow flow vascular malformations that are associated with identical *PIK3CA* GOF mutations[36–38], and newer agents directly targeting PIK3CA itself have also been found to be effective for treatment of inoperable vascular malformations associated with *PIK3CA* GOF mutations[39]. It is reasonable to predict that such drugs will also be effective for treatment of aggressive CCM lesions.

Online content

Any methods, additional references, Nature Research reporting summaries, source data, extended data, supplementary information,

acknowledgements, peer review information; details of author contributions and competing interests; and statements of data and code availability are available at https://doi.org/10.1038/s41586-021-03562-8.

1. Cuttano, R. *et al*. KLF4 is a key determinant in the development and progression of cerebral cavernous malformations. *EMBO Mol Med*, https://doi.org/10.15252/emmm.201505433 (2015).
2. Zhou, Z. *et al*. Cerebral cavernous malformations arise from endothelial gain of MEKK3-KLF2/4 signalling. *Nature* **532**, 122-126, https://doi.org/10.1038/nature17178 (2016).
3. Renz, M. *et al*. Regulation of beta1 integrin-Klf2-mediated angiogenesis by CCM proteins. *Dev Cell* **32**, 181-190, https://doi.org/10.1016/j.devcel.2014.12.016 (2015).
4. Otten, C. *et al*. Systematic pharmacological screens uncover novel pathways involved in cerebral cavernous malformations. *EMBO Mol Med* **10**, https://doi.org/10.15252/emmm.201809155 (2018).
5. Tang, A. T. *et al*. Endothelial TLR4 and the microbiome drive cerebral cavernous malformations. *Nature* **545**, 305-310, https://doi.org/10.1038/nature22075 (2017).
6. Fischer, A., Zalvide, J., Faurobert, E., Albiges-Rizo, C. & Tournier-Lasserve, E. Cerebral cavernous malformations: from CCM genes to endothelial cell homeostasis. *Trends Mol Med* **19**, 302-308, https://doi.org/10.1016/j.molmed.2013.02.004 (2013).
7. Fisher, O. S. & Boggon, T. J. Signaling pathways and the cerebral cavernous malformations proteins: lessons from structural biology. *Cellular and molecular life sciences : CMLS* **71**, 1881-1892, https://doi.org/10.1007/s00018-013-1532-9 (2014).
8. Plummer, N. W., Zawistowski, J. S. & Marchuk, D. A. Genetics of cerebral cavernous malformations. *Curr Neurol Neurosci Rep* **5**, 391-396 (2005).
9. Al-Shahi Salman, R. *et al*. Untreated clinical course of cerebral cavernous malformations: a prospective, population-based cohort study. *Lancet Neurol* **11**, 217-224, https://doi.org/10.1016/S1474-4422(12)70004-2 (2012).
10. Awad, I. A. & Polster, S. P. Cavernous angiomas: deconstructing a neurosurgical disease. *J Neurosurg* **131**, 1-13, https://doi.org/10.3171/2019.3.JNS181724 (2019).
11. Porter, P. J., Willinsky, R. A., Harper, W. & Wallace, M. C. Cerebral cavernous malformations: natural history and prognosis after clinical deterioration with or without hemorrhage. *J Neurosurg* **87**, 190-197, https://doi.org/10.3171/jns.1997.87.2.0190 (1997).
12. Boulday, G. *et al*. Developmental timing of CCM2 loss influences cerebral cavernous malformations in mice. *J Exp Med*, jem.20110571 [pii] https://doi.org/10.1084/jem.20110571 (2011).
13. Maddaluno, L. *et al*. EndMT contributes to the onset and progression of cerebral cavernous malformations. *Nature* **498**, 492-496, nature12207 [pii] https://doi.org/10.1038/nature12207 (2013).
14. Detter, M. R., Snellings, D. A. & Marchuk, D. A. Cerebral Cavernous Malformations Develop Through Clonal Expansion of Mutant Endothelial Cells. *Circ Res* **123**, 1143-1151, https://doi.org/10.1161/CIRCRESAHA.118.313970 (2018).
15. Malinverno, M. *et al*. Endothelial cell clonal expansion in the development of cerebral cavernous malformations. *Nat Commun* **10**, 2761, https://doi.org/10.1038/s41467-019-10707-x (2019).
16. Ramirez-Zamora, A. & Biller, J. Brainstem cavernous malformations: a review with two case reports. *Arq Neuropsiquiatr* **67**, 917-921, https://doi.org/10.1590/s0004-282x2009000500030 (2009).
17. Castro, M. *et al*. CDC42 Deletion Elicits Cerebral Vascular Malformations via Increased MEKK3-Dependent KLF4 Expression. *Circ Res* **124**, 1240-1252, https://doi.org/10.1161/CIRCRESAHA.118.314300 (2019).
18. Hong, C. C. *et al*. Cerebral cavernous malformations are driven by ADAMTS5 proteolysis of versican. *J Exp Med* **217**, https://doi.org/10.1084/jem.20200140 (2020).
19. Lissbrant, I. F., Lissbrant, E., Persson, A., Damber, J. E. & Bergh, A. Endothelial cell proliferation in male reproductive organs of adult rat is high and regulated by testicular factors. *Biol Reprod* **68**, 1107-1111, https://doi.org/10.1095/biolreprod.102.008284 (2003).
20. Samuels, Y. *et al*. Mutant PIK3CA promotes cell growth and invasion of human cancer cells. *Cancer Cell* **7**, 561-573, https://doi.org/10.1016/j.ccr.2005.05.014 (2005).
21. Rodriguez-Laguna, L. *et al*. Somatic activating mutations in PIK3CA cause generalized lymphatic anomaly. *J Exp Med* **216**, 407-418, https://doi.org/10.1084/jem.20181353 (2019).
22. Castillo, S. D. *et al*. Somatic activating mutations in Pik3ca cause sporadic venous malformations in mice and humans. *Sci Transl Med* **8**, 332ra343, https://doi.org/10.1126/scitranslmed.aad9982 (2016).
23. Castel, P. *et al*. Somatic PIK3CA mutations as a driver of sporadic venous malformations. *Sci Transl Med* **8**, 332ra342, https://doi.org/10.1126/scitranslmed.aaf1164 (2016).
24. Luks, V. L. *et al*. Lymphatic and other vascular malformative/overgrowth disorders are caused by somatic mutations in PIK3CA. *J Pediatr* **166**, 1048-1054 e1041-1045, https://doi.org/10.1016/j.jpeds.2014.12.069 (2015).
25. Limaye, N. *et al*. Somatic Activating PIK3CA Mutations Cause Venous Malformation. *Am J Hum Genet* **97**, 914-921, https://doi.org/10.1016/j.ajhg.2015.11.011 (2015).
26. Storck, S. E. *et al*. Endothelial LRP1 transports amyloid-beta(1-42) across the blood-brain barrier. *J Clin Invest* **126**, 123-136, https://doi.org/10.1172/JCI81108 (2016).
27. Rigamonti, D. *et al*. Cerebral cavernous malformations. Incidence and familial occurrence. *N Engl J Med* **319**, 343-347 (1988).
28. Dogruluk, T. *et al*. Identification of Variant-Specific Functions of PIK3CA by Rapid Phenotyping of Rare Mutations. *Cancer Res* **75**, 5341-5354, https://doi.org/10.1158/0008-5472.CAN-15-1654 (2015).
29. Gault, J., Shenkar, R., Recksiek, P. & Awad, I. A. Biallelic somatic and germ line CCM1 truncating mutations in a cerebral cavernous malformation lesion. *Stroke* **36**, 872-874, 01.STR.0000157586.20479.fd [pii] https://doi.org/10.1161/01.STR.0000157586.20479.fd (2005).
30. Akers, A. L., Johnson, E., Steinberg, G. K., Zabramski, J. M. & Marchuk, D. A. Biallelic somatic and germline mutations in cerebral cavernous malformations (CCMs): evidence for a two-hit mechanism of CCM pathogenesis. *Hum Mol Genet* **18**, 919-930, ddn430 [pii] https://doi.org/10.1093/hmg/ddn430 (2009).
31. McDonald, D. A. *et al*. Lesions from patients with sporadic cerebral cavernous malformations harbor somatic mutations in the CCM genes: evidence for a common biochemical pathway for CCM pathogenesis. *Hum Mol Genet* **23**, 4357-4370, https://doi.org/10.1093/hmg/ddu153 (2014).
32. Xu, L. *et al*. Clonal Evolution and Changes in Two AML Patients Detected with A Novel Single-Cell DNA Sequencing Platform. *Sci Rep* **9**, 11119, https://doi.org/10.1038/s41598-019-47297-z (2019).
33. Lopez-Ramirez, M. A. *et al*. Thrombospondin1 (TSP1) replacement prevents cerebral cavernous malformations. *J Exp Med* **214**, 3331-3346, https://doi.org/10.1084/jem.20171178 (2017).
34. Abdulrauf, S. I., Kaynar, M. Y. & Awad, I. A. A comparison of the clinical profile of cavernous malformations with and without associated venous malformations. *Neurosurgery* **44**, 41-46; discussion 46-47, https://doi.org/10.1097/00006123-199901000-00020 (1999).
35. Tan, W. H. *et al*. The spectrum of vascular anomalies in patients with PTEN mutations: implications for diagnosis and management. *J Med Genet* **44**, 594-602, https://doi.org/10.1136/jmg.2007.048934 (2007).
36. Adams, D. M. *et al*. Efficacy and Safety of Sirolimus in the Treatment of Complicated Vascular Anomalies. *Pediatrics* **137**, e20153257, https://doi.org/10.1542/peds.2015-3257 (2016).
37. Ozeki, M. *et al*. The impact of sirolimus therapy on lesion size, clinical symptoms, and quality of life of patients with lymphatic anomalies. *Orphanet J Rare Dis* **14**, 141, https://doi.org/10.1186/s13023-019-1118-1 (2019).
38. Triana, P. *et al*. Sirolimus in the Treatment of Vascular Anomalies. *Eur J Pediatr Surg* **27**, 86-90, https://doi.org/10.1055/s-0036-1593383 (2017).
39. Venot, Q. *et al*. Targeted therapy in patients with PIK3CA-related overgrowth syndrome. *Nature* **558**, 540-546, https://doi.org/10.1038/s41586-018-0217-9 (2018).

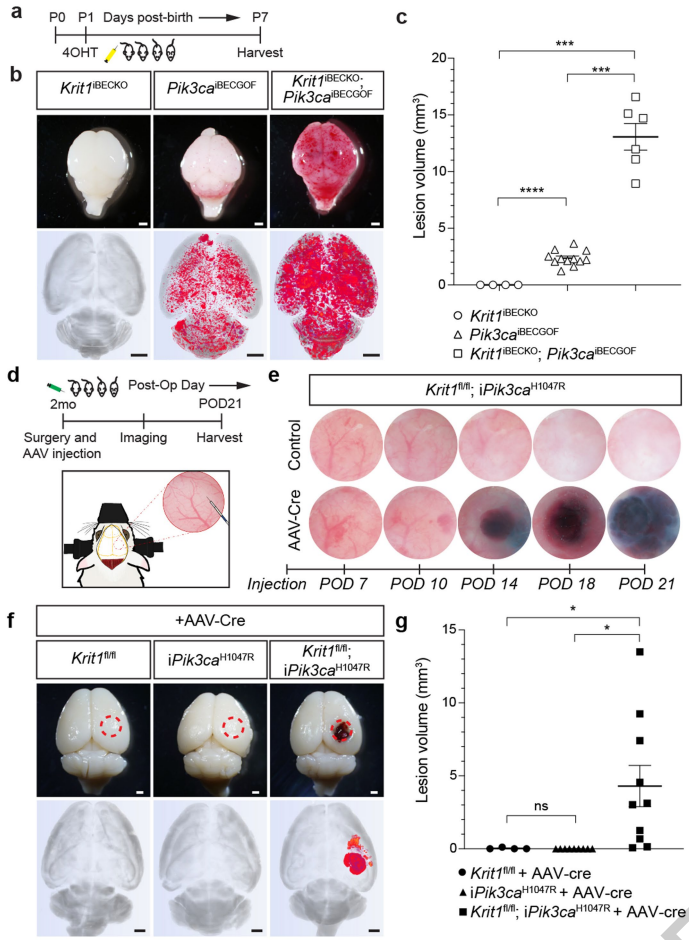

Fig. 1 | CCM LOF and PIK3CA GOF synergize during cavernous malformation in the neonatal brain and are both required for malformations in the adult brain. a, Schematic of neonatal induction of *Krit1* deletion and/or PIK3CA^{H1047R} expression. 4-hydroxytamoxifen (4OHT) injection at P1 was used to inducibly delete *Krit1* (*Krit1*^{iBECKO}), drive expression of PIK3CA^{H1047R} (*Pik3ca*^{iBECGOF}) or both specifically in the brain endothelial cells of mice carrying a resistant gut microbiome. **b**, Representative visual and microCT images of the indicated P7 brains. Note that loss of KRIT1 alone is not sufficient for CCM formation in animals with a resistant microbiome. Scale bars, 1mm. **c**, MicroCT quantitation of lesion volumes at P7. (*Krit1*^{iBECKO}, *n*=4; *Pik3ca*^{iBECGOF}, *n*=12; *Krit1*^{iBECKO};*Pik3ca*^{iBECGOF}, *n*=6). Indicated p-values are: p=0.0002; p=0.0001; p=8e^{-8} (top to bottom). **d**, Schematic and diagram of the experimental approach in which a cranial window is created and AAV virus injected into the brains of 2 month old mice with serial imaging on indicated post-operative days (POD). **e**, Serial images obtained through the same cranial window of *Krit1*$^{fl/fl}$;i*Pik3ca*^{H1047R} animals following injection of control or Cre-expressing AAV vectors. Cranial window images representative of 4 animals/group. **f**, Representative visual and microCT images of brains harvested 21 days after injection of AAV-Cre into adult animals with the indicated genotypes. i*Pik3ca*^{H1047R} designation includes i*Pik3ca*^{H1047R} and/or *Krit1*$^{fl/+}$;i*Pik3ca*^{H1047R} genotypes. Dotted circles indicate the site of cranial window and AAV-Cre injection. Scale bars, 1mm. **g**, MicroCT quantitation of lesion volumes 21 days after injection of AAV-Cre. (*Krit1*$^{fl/fl}$, *n*=4; i*Pik3ca*^{H1047R}, *n*=9; *Krit1*$^{fl/fl}$;i*Pik3ca*^{H1047R}, *n*=10). Indicated p-values are: p=0.0144; p=0.0140; p=0.4174 (top to bottom). Data are mean ± s.e.m. Unpaired, two-tailed Welch's t-test. ns indicates p not significant, p>0.05; *indicates p<0.05; ***indicates p<0.001; ****indicates p<0.0001.

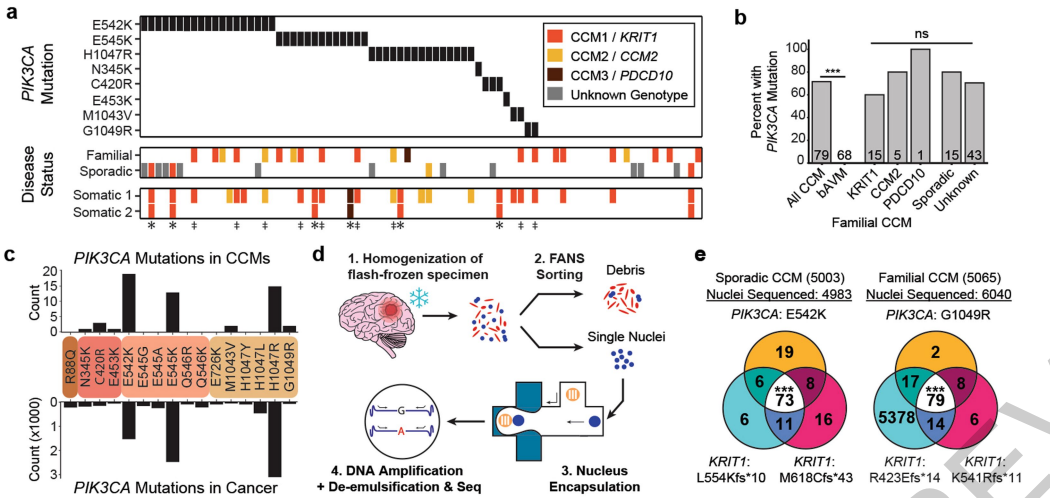

Fig. 2 | GOF *PIK3CA* mutations and LOF CCM gene mutations co-exist in the same cell in human CCMs. a, A schematic summary of the somatic *PIK3CA* mutations, the germline mutations in *KRIT1*, *CCM2* and *PDCD10*, and the somatic mutations in *KRIT1*, *CCM2* and *PDCD10* as identified in 79 human CCMs via bulk sequencing of frozen resected tissue is shown. Color denotes the affected CCM gene. Samples listed as neither familial nor sporadic are deidentified banked CCMs lacking either clinical information or genetic evidence supporting either classification. ‡ indicates familial CCMs with an activating mutation in *PIK3CA* and both germline and somatic mutations in a CCM gene. * indicates known or presumed sporadic CCMs with an activating mutation in *PIK3CA* and two somatic mutations in a CCM gene. **b**, Percentage of lesions with an activating mutation in *PIK3CA* present in all sequenced CCMs vs. control brain AVMs, all three forms of familial CCMs and sporadic CCMs. The value inside the bar shows the number of samples in the corresponding group. **c**, The distributions of the 16 most common somatic *PIK3CA* mutations identified in human CCMs (top) and cancer (bottom) as reported in the COSMIC database are shown. Colored boxes represent domains in *PIK3CA* in order from left to right: Adaptor BD, RAS BD, C2, Kinase. **d**, Schematic of workflow for processing frozen surgically-resected human CCM lesions for single-nucleus DNA sequencing. **e**, Representative data for sporadic and familial CCMs detailing the number of nuclei with each combination of *PIK3CA* and CCM mutations. p was determined by two-tailed chi-squared test between the observed and expected triple mutant nuclei predicted by a Poisson distribution (see Methods). ns indicates p not significant, p>0.05; ***indicates $p<1e^{-16}$.

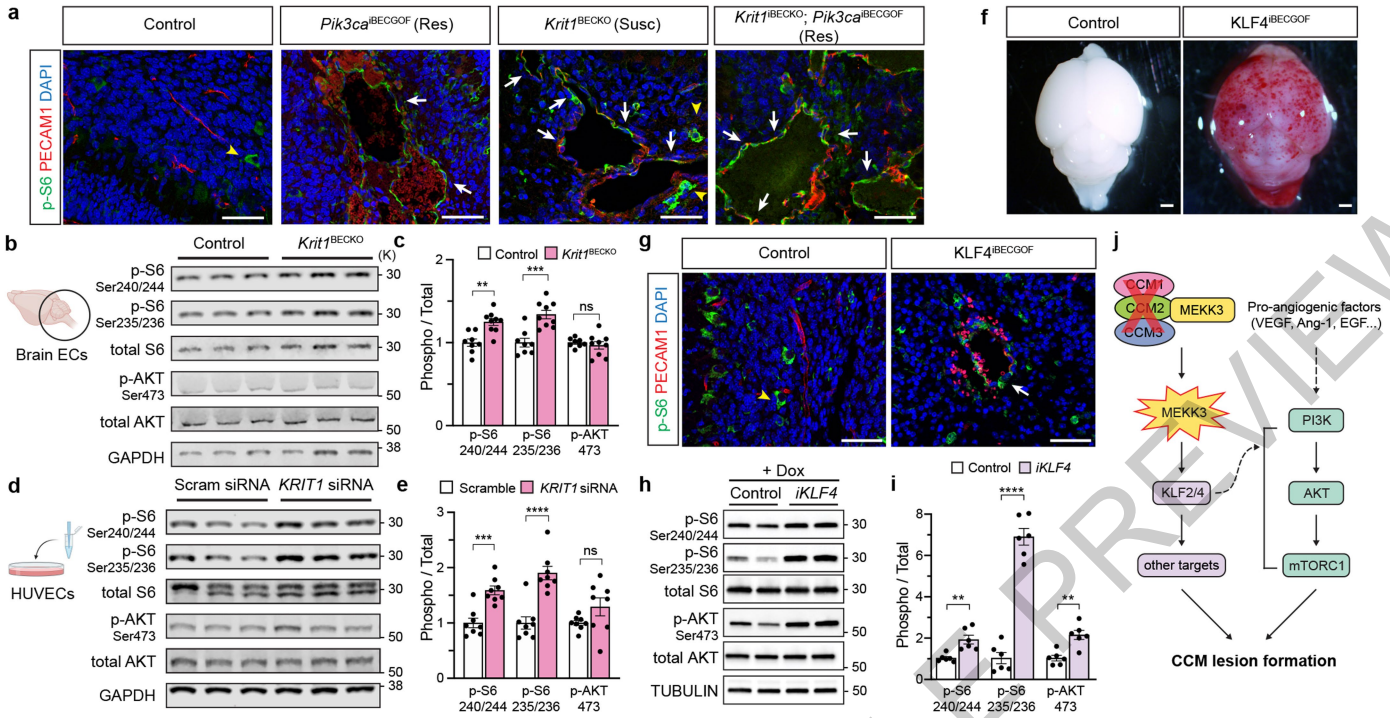

Fig. 3 | Endothelial CCM LOF augments PI3K-mTORC1 signaling through KLF4. a, Immunostaining for phospho-S6 ribosomal protein (p-S6) and endothelial cell (EC) marker PECAM1 in P6 hindbrain sections with a resistant (Res) or susceptible (Susc) microbiome. White arrows indicate p-S6 positive ECs, yellow arrowheads indicate non-endothelial p-S6 positive cells in **a** and **g**. Scale bars, 50 microns. **b**, Immunoblot detection of phospho-AKT (p-AKT) and p-S6 in ECs from the hindbrains of P6 control and *Krit1*^{BECKO} littermates. GAPDH loading control. **c**, Quantitation of immunoblotting for p-AKT and p-S6 relative to total AKT and S6 protein. (*n*=8 hindbrains/group) Indicated p-values are: p=0.0010; p=0.0003; p=0.5205 (left to right). **d**, Immunoblot detection of p-AKT and p-S6 in cultured HUVECs treated with scrambled or *KRIT1* siRNAs. **e**, Quantitation of immunoblotting for p-AKT and p-S6 relative to total AKT and S6 protein. (*n*=8 individual wells/group over 4 independent experiments). Indicated p-values are: p=0.0002; p=7e^{-6}; p=0.1208 (left to right). **f**, Visual images of P6 control and KLF4^{iBECGOF} littermates. Images representative of 8 animals/group. Scale bars, 1mm. **g**, Immunostaining for p-S6 and PECAM1 in hindbrain sections from P6 control and KLF4^{iBECGOF} littermates. Scale bars, 50 microns. **h**, Immunoblot detection of p-AKT and p-S6 in HUVECs with expression of KLF4-GFP ("i*KLF4*" cells) or control lentivirus. Tubulin loading control. **i**, Quantitation of immunoblotting for p-AKT and p-S6 relative to total AKT and S6 in control and i*KLF4* HUVECs. (*n*=6 individual wells/group over 3 independent experiments). p=0.0067; p=9e^{-7}; p=0.0022 (left to right). **j**, Pathway schematic of how gain of CCM-MEKK3-KLF2/4 signaling is proposed to augment PI3K-mTORC1 signaling to drive CCM formation. Immunofluorescence in **a** and **g** representative of 10 tissue sections from *n*=4 individual animals/genotype. Data are mean ± s.e.m. Unpaired, two-tailed Welch's t-test. ns indicates p not significant, p>0.05; **indicates p<0.01; ***indicates p<0.001; ****indicates p<0.0001. For gel source data, see Supplementary Figure 1.

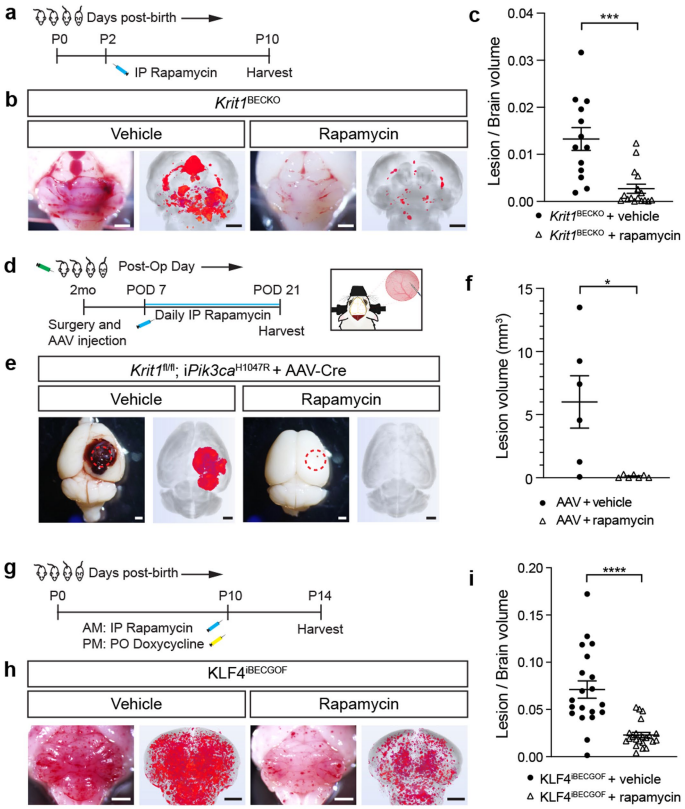

Fig. 4 | Rapamycin prevents lesion formation due to CCM LOF and KLF4 GOF in neonatal and adult mice. a, Schematic of neonatal *Krit1*^{BECKO} animals with a susceptible microbiome administered a single dose treatment with Rapamycin or vehicle on P2. **b**, Representative visual and microCT images of the hindbrains of littermates treated with either vehicle or Rapamycin. Scale bars, 1mm. **c**, MicroCT quantitation of lesion volumes normalized to total brain volume following treatment with vehicle or Rapamycin. (Vehicle, *n*=13; Rapamycin, *n*=16). p=0.0009. **d**, Experimental design for Rapamycin or vehicle treatment of adult animals with combined CCM LOF and PIK3CA GOF (*Krit1*$^{fl/fl}$;*iPik3ca*^{H1047R}) using cranial window surgery and AAV injection is shown. **e**, Representative visual and microCT images of brains harvested 21 days after injection of AAV-Cre into littermate animals. Dotted circles indicate the site of cranial window and AAV-Cre injection. Scale bars, 1mm. **f**, MicroCT quantitation of lesion volumes 21 days after creation of the cranial window and injection of AAV-Cre is shown. (Vehicle, *n*=6; Rapamycin, *n*=7). p=0.0358. **g**, Schematic of neonatal KLF4^{iBECGOF} animals administered a single dose treatment with Rapamycin or vehicle followed by induction of KLF4 expression on P10. **h**, Representative visual and microCT images of the hindbrains of littermates treated with either vehicle or Rapamycin. Scale bars, 1mm. **i**, MicroCT quantitation of lesion volumes normalized to total brain volume following treatment of the indicated mice with vehicle or Rapamycin. (Vehicle, *n*=20; Rapamycin, *n*=22). p=4e^{-5}. Data are mean ± s.e.m. Unpaired, two-tailed Welch's t-test. *indicates p<0.05; ***indicates p<0.001; ****indicates p<0.0001.

Methods

Mice

Cdh5-CreERT2[40], *Slco1c1*(BAC)-Cre[41] *Slco1c1*(BAC)-CreERT2[41], *Pdgfb*-CreERT2,[42] *Krit1*$^{fl/fl}$[43], tetOn-KLF4[44], and *Pten*$^{fl/fl}$[45] animals have been previously described. R26-nTnG (JAX #023035), R26-LSL-*Pik3ca*^{H1047R} (JAX#016977 and[46]) animals were obtained from the Jackson Laboratories. R26-CAGs-LSL-rtTA3 mice (JAX#029617) were generously provided by Lukas Dow. All experimental animals were maintained on a mixed-strain background and littermate controls were used for neonatal experiments unless otherwise indicated. Breeding pairs between 2 and 8 months of age were used to generate the neonatal CCM mouse model of the indicated genotypes. Sample size was determined by prior studies using similar animals and techniques.

For all neonatal CCM experiments utilizing the *Cdh5*-CreERT2; *Krit1*$^{fl/fl}$ ("*Krit1*^{iECKO}"), *Slco1c1*(BAC)-CreERT2;*Krit1*$^{fl/fl}$ ("*Krit1*^{iBECKO}"), *Slco1c1*(BAC)-Cre;*Krit1*$^{fl/fl}$ ("*Krit1*^{BECKO}") models, P1 pups were injected intra-gastrically by a 30-gauge needle with 40 µg of 4-hydroxytamoxifen (4OHT, Sigma Aldrich, H7904) dissolved in 9% ethanol/corn oil vehicle (50 µl total volume per injection). The solution was freshly prepared from pre-measured, 4OHT powder for every injection. The P1 time point was defined by checking experimental breeding pairs every evening for new litters. The following morning (P1), pups were injected with 4OHT in a blinded fashion without knowledge of genotypes. Pups were then harvested, as previously described[2], at specified time points.

For adult CCM deletion experiments utilizing littermate *Cdh5*-CreERT2;*Krit1*$^{fl/fl}$ ("*Krit1*^{iECKO}") animals, tamoxifen (Sigma Aldrich, T564) was dissolved in a 100% corn oil vehicle. The solution was freshly prepared for every gavage. Male mice were given 3mg tamoxifen via gavage beginning at two months of age, twice a week for three weeks, for a total of six gavages, then placed on tamoxifen chow diet (Envigo, TD.160410) until harvested at six months of age.

For craniotomy experiments, adult mice of the genotypes *Krit1*$^{fl/fl}$, *Krit1*$^{fl/+}$;R26-LSL-*Pik3ca*^{H1047R}, or *Krit1*$^{fl/fl}$; R26-LSL-*Pik3ca*^{H1047R} of either gender, between 6-10 weeks of age were used.

For KLF4 GOF experiments utilizing *Slco1c1*(BAC)-Cre; R26-LSL-rtTA;tetO-KLF4 ("KLF4^{iBECGOF}") animals, P1 pups were intra-gastrically injected by a 31G insulin syringe with 200 µg of doxycycline (Sigma-Aldrich, D9891) dissolved in PBS (20 µl total volume per injection). Pups were harvested at P6 unless otherwise indicated.

All mice were housed in individual, ventilated cages with 12-hr light/dark cycles with food and water ad libitum. All animals were housed in a pathogen-free environment in an AAALAC-approved vivarium at the University of Pennsylvania, and experiments were performed in accordance with the guidelines of the Institutional Animal Care and Use Committee (IACUC).

Histology, immunohistochemistry and quantification

Mice were anesthetized with IP injection of tribromoethanol (Avertin), followed by intracardial perfusion with 20mL of cold PBS and 4% (w/v) paraformaldehyde (PFA) in PBS (pH 7.4) for adult mice and 10ml respectively for neonates. Tissue samples were fixed in 4% PFA/PBS overnight at 4 °C, dehydrated to 100% ethanol, and embedded in paraffin. Tissue sections of 6 µm underwent dewaxing and rehydration through xylene and ethanol treatment and were subsequently used for haematoxylin and eosin (H-E) and immunohistochemistry staining. For immunodetection, 10mM citrate buffer (pH 6) (Sigma - C9999) was used for antigen retrieval, and sections were blocked with 10% donkey serum in 1% BSA prior to primary antibody treatment overnight at 4 °C. The following primary antibodies were used for immunostaining: rat anti-PECAM1/CD31 (1:200; HistoBioTec, DIA-310), goat anti-KLF4 (1:100; R&D Systems, AF3158), goat anti-GFP (1:100; Rockland Immunochemicals, 600-101-215), rabbit anti-ERG (1:100; Abcam, ab110639), rabbit anti-phospho-S6 (1:200, Cell Signaling Technologies, 4858S). Fluorescence-conjugated Alexa Fluor secondary antibodies were used (1:500, Invitrogen) according to the primary antibody species and counterstained with DAPI (1:1000). Secondary antibodies were validated for non-specific staining by no primary antibody negative controls.

Control and experimental animal sections were stained at the same time under identical conditions. Sections were mounted on slides with ProLong Gold Antifade reagent. Images were acquired on a Nikon 80i Eclipse, an Olympus DP80 microscope, and/or Zeiss LSM 710 or Zeiss 880 Confocal microscope at the same exposure times, using x4, x10, x20, and x40 objectives, and subsequently processed in ImageJ software (NIH).

Quantification for the R26-nTnG leak experiment was done by counting the number of nGFP-positive, ERG-positive endothelial over total number of ERG-positive cells present within a lesion. 20 random 800um x 800um -fields, from three unique individual animals were assessed.

Isolation of cerebellar endothelial cells

At the specified time points, cerebellar endothelial cells were isolated by mechanical and enzymatic digestion followed by separation using magnetic-activated cell sorting by anti-CD31/PECAM1-conjugated magnetic beads (MACS MS system, Miltenyi Biotec), as previously described[2].

siRNA knockdown and lentiviral expression in cultured endothelial cells

Cell culture: Pooled human umbilical vein endothelial cells (HUVECs) were purchased from Lonza (#CC- 5 2519) and cultured in endothelial basal medium (EBM, Lonza) supplemented with hydrocortisone (1µg/ml), bovine brain extract (12 µg/ml), gentamicin (50 µg/ml), human recombinant epidermal growth factor (10 ng/ml), and 10% fetal bovine serum (FBS, Life Technologies). HUVECs were tested negative for mycoplasma and cultured until the fourth passage. Cells were maintained at 37° C in a humidified atmosphere with 5% CO2.

siRNAs directed against *KRIT1* (s2510, Invitrogen) were used for the knockdown experiments at a concentration of 10nM. For overexpression studies, HUVECs were infected with a control lentivirus encoding either GFP, or mutant human *PIK3CA* with the H1047R mutation (constructed from pBabe puro HA PIK3CA H1047R from Jean Zhao (Addgene plasmid # 12524). Cells were harvested 48 hours post-infection or post-transfection and total RNA was isolated using TRIzol Reagent (Life Technologies). cDNA was generated from 500ng total RNA using the SuperScript IV VILO Master Mix (Thermo Fisher, 11756050) and real time qPCR was performed using Power SYBR Green PCR Master Mix (Applied Biosciences). Protein was harvested with RIPA buffer with complete protease inhibitor cocktail (Roche) and PhosSTOP phosphatase inhibitor cocktail (Roche).

Human primers:
GAPDH forward: 5′-CTGGGCTACACTGAGCACC-3′
GAPDH reverse: 5′-AAGTGGTCGTTGAGGGCAATG-3′
KLF2 forward: 5′-CTACACCAAGAGTTCGCATCTG-3′
KLF2 reverse: 5′-CCGTGTGCTTTCGGTAGTG-3′
KLF4 forward: 5′-AGAGTTCCCATCTCAAGGCA -3′
KLF4 reverse: 5′-GTCAGTTCATCTGAGCGGG -3′
PIK3CA forward: 5′- CCACGACCATCATCAGGTGAA-3′
PIK3CA reverse: 5′- CCTCACGGAGGCATTCTAAAGT-3′

Lentivirus generation, production and infection

For doxycycline-inducible lentiviral expression of a human GFP-tagged KLF4 (isoform 1) cDNA was cloned into pLVX-TetOne-Puro (Clontech). Virus production was performed by co-transfecting pMD2.G (Addgene, #12259), psPAX2 (Addgene, #12260) and transfer plasmids into HEK293FT cells. Transfections were performed with the Lipofectamine 2000 transfection reagent (Life Technologies) according to the manufacturer's instructions. Viruses were harvested after 24 and 48 hours and then incubated with HUVECs for 16 hours in the presence of 8 µg/ml polybrene (Santa Cruz Biotechnology, #SC-134220). Fresh

EBM media containing 1 µg/ml puromycin (InvivoGen, #ant-pr-1) was added to select transduced cells. To induce KLF4 expression, selected cells were treated with 300ng/mL doxycycline for 72 hours before harvesting. Lentiviruses encoding for GFP were used as a control.

Gene expression analysis from isolated endothelial cells

Total RNA was extracted from isolated endothelial cells using the RNEasy Mini Kit (Qiagen) and reverse transcribed using the SuperScript IV VILO Master Mix (Thermo Fisher, 11756050). To quantify transcript expression levels, real-time PCR was performed using Power SYBR Green PCR Master Mix (Thermo Fisher, 4368577). Relative gene expression was normalized to *Gapdh* levels and calculated using the ddCt method. The following mouse primers sequences were used:

Mouse primers:
Gapdh forward: 5′-AAATGGTGAAGGTCGGTGTGAACG-3′
Gapdh reverse: 5′-ATCTCCACTTTGCCACTGC-3′
Klf2 forward: 5′-CGCCTCGGGTTCATTTC-3′
Klf2 reverse: 5′-AGCCTATCTTGCCGTCCTTT-3′
Klf4 forward: 5′-GTGCCCCGACTAACCGTTG-3′
Klf4 reverse: 5′-GTCGTTGAACTCCTCGGTCT-3′
Pik3ca forward: 5′- CCACGACCATCTTCGGGTG-3′
Pik3ca reverse: 5′- GGGGAGTAAACATTCCACTAGGA-3′

Immunoblotting of protein from isolated or cultured endothelial cells

Western blot analyses were performed with precast gradient gels (Bio-Rad) using standard methods. Briefly, HUVECs were lysed in RIPA buffer (Sigma; 150 mM NaCl, 1.0% (v/v) IGEPAL CA-630, 0.5% sodium deoxycholate, 0.1% SDS, and 50 mM Tris, pH 8.0) supplemented with 1× EDTA-Free Complete Protease Inhibitor Cocktail (Roche) and 1 mM phenylmethylsulfonyl fluoride. Proteins were separated by SDS-PAGE (Tris-glycine gels with Tris/glycine/SDS buffer, Bio-Rad) and transferred onto nitrocellulose membranes using the Trans Turbo Blot system (Bio-Rad). Membranes were probed with specific primary antibodies and then with peroxidase-conjugated secondary antibodies. The following antibodies were used for immunoblotting: rabbit anti-GAPDH (1:2,000, Cell Signaling Technologies, 2118), rabbit anti-phospho-AKT Ser 473 (1:1000, Cell Signaling Technologies, 4060), rabbit anti-phospho-S6 Ser 235/236 (1:1000, Cell Signaling Technologies, 4858), mouse anti-total AKT (1:1000, Cell Signaling Technologies, 2920) and mouse anti-total S6 (1:1000, Cell Signaling Technologies, 2317). For the immunoblots shown, the following antibodies were used: eNOS (Cell Signaling Technology, #9586, 1:1000), GFP (Cell Signaling Technology, #2555, 1:5000), KLF4 (Cell Signaling Technology, #4038, 1:1000), Phospho-S6 (Ser 235/236) Ribosomal protein (Cell Signaling Technology, #4857, 1:4000), Phospho-S6 (Ser 240/244) Ribosomal protein (Cell Signaling Technology, #2215, 1:4000), S6-Ribosomal protein (Cell Signaling Technology, #2217, 1:4000), Phospho-AKT (Ser 473) (Cell Signaling Technology, #4060, 1:2000), Phospho-AKT (Thr 308) (Cell Signaling Technology, #4056, 1:1000), AKT (pan) (Cell Signaling Technology, #4685, 1:2000), Tubulin (Cell Signaling Technology, #2148, 1:5000). Secondary antibodies are peroxidase-conjugated Goat IgGs (1:5000) purchased from Jackson Immuno Research Labs. Quantification was normalized to total protein. Imaging was performed on a Licor Odyssey FC system and quantified using ImageStudio software.

X-ray microCT-based quantification of CCM lesions

For all experiments using microCT quantification of CCM lesion volume, brains were harvested and placed in 4% PFA/PBS. Brains remained in fixative until staining with non-destructive, iodine contrast and subsequent microCT imaging performed as previously described[5]. Tissue processing, imaging, and volume quantification were performed in a blinded manner by investigators at the University of Chicago without any knowledge of genotype and experimental details.

Craniotomy survival surgery

Animals were anesthetized with isoflurane (3% induction, 1-2% maintenance in 1L/min oxygen) for surgery. Mice were placed on heating pad covered with cotton pad to maintain body temperature of 37.5C. Depth of anesthesia was periodically monitored by testing the animal's reflex through toe pinch. Eyes were covered with ophthalmic lubricant to prevent drying. A stereotactic frame (Stoeling Instruments) was used to immobilize the head using ear bars. All mice receiving craniotomies also received 1.5mg/kg of dexamethasone intramuscularly (Sigma) and 5mg/kg of 10% meloxicam (Midwest Vet Supply) subcutaneously.

After the head is immobilized, hair on the scalp was removed with Nair. The scalp was subsequently cleaned and sterilized with 70% ethanol and betadine at least three times. A midline scalp incision was made and resected to expose the skull. The periosteum was removed with blunt forceps. The outer table of the skull was thinned using a handheld high-speed dental drill (Foredom) using a 0.5mm burr. In the adult mice, a 3-4mm^2 circumferential region was chosen over the right somatosensory cortex posterior to the coronal suture. Sterile saline was used to irrigate the drill burr to prevent build-up of bone residue and heating of the drill bit. Gelfoam in sterile saline was used to provide hemostasis and to remove bone dust. The border of the craniotomy was thinned until the inner table fractures. A fine-tip forcep (Fine Science Tools) or an up-angled curette (Fine Science Tools) can be used to lift the bone flap and gently elevate it from the dura. Gelfoam was used to provide hemostasis and prevent the brain surface from desiccating.

Upon completion of intraparenchymal viral injection, hemostasis was obtained. A cranial window made from #0 3mm coverslip cemented to a #0 5mm coverslip (Warner) was then placed over the craniotomy site and secured to the skull using cyanoacrylate glue. A custom-made imaging rig (3D printed using ABS) was then secured over the glass coverslip using cyanoacrylate glue and dental cement (Metabond).

Post-surgery, adult mice were monitored and kept separately from littermates until awake and mobile. Mice who developed any post-operative seizures were euthanized. A second dose of subcutaneous meloxicam was given to mice as necessary based on a second exam an hour after surgery. Mice were monitored and imaged for up to 21 days after AAV injection before they were harvested.

Adeno-associated virus injection

Recombinant AAV vectors were generously donated by the lab of Jakob Körbelin[47]. AAV-BR1 vectors carrying Cre recombinase under the control of the CAG promoter vector was injected into the right lateral hemisphere of mice using a beveled glass micropipette. 100nL of 5 x 10^7 virus particles in sterile PBS was injected over the course of 5 minutes.

Lineage tracing AAV-Cre following intracranial injection of adult mice

Mice were housed in individually ventilated Green Line cages (Tecniplast) under a 12-hour light/dark cycle and fed an autoclaved pelleted mouse diet *ad libitum*. 12 weeks old Ai14 mice were stereotactic injected into the cortex with the AAV-BR1-CAG-Cre (2x10^9 gp; 200nl). Mice were anesthetized with an intraperitoneal (i.p.) injection of a mixture of ketamine hydrochloride (65 µg g^{-1} body weight) and xylazine (15 µg g^{-1} body weight) in NaCl (0.9%). After loss of reflexes, animals were fixed in a stereotaxic frame (David Kopf instruments; Nr: 1900). The following coordinates relative to bregma were used for injections: lateral ventricle, anteroposterior −0,1,5 mm, mediolateral −0.75 mm, dorsoventral from the skull surface −2.0 mm. A small hole was made into the skull using a dental drill (freedom; K.1070 Micromotor Kit). After injection, the micropipette was kept in place for 5 min to avoid backflow of the injected vector during micropipette retraction. The scalp was sutured, and the animals were placed on a heating pad until full recovery from surgery and then returned to their home cage. Carprofen (5 mg kg^{-1} body weight; s.c.) was applied once a day for 2 days after rAAV injection.

Two weeks after viral injection, mice were perfused with Ringer solution and afterwards with 4% paraformaldehyde (PFA) during deep aesthesia. Brains were postfixed in 4% PFA at 4 °C overnight. Sections (50 µm) were prepared with a vibratome. Free-floating sections were washed twice in PBS, permeabilized with 0.3% Triton X-100 in PBS (PBS-TX) for 30 min, and incubated in bovine serum albumin (5% in PBS-TX) for 2 h. Primary antibodies (anti-CD31, Bio Rad (MCA2388) 1:200 (5 µg/ml) in BSA-PBS-TX) were added followed by overnight incubation with gently shaking. Sections were washed twice in PBS-TX for 10 min and incubated for 2 h with secondary antibodies (anti-rat IgG (Alexa Fluor 488), ThermoFisher (A-21208), 1:400 (5 µg/ml) in BSA-PBS-TX). After washing twice in PBS, sections were incubated with DAPI (1 µg/ml in PBS) for 5 min and washed twice in PBS for 5 min. Then, sections were mounted on glass slides and covered with Mowiol.

Rapamycin injection

Rapamycin (MedChemExpress, HY-10219) was dissolved in DMSO for a 10mg/ml stock solution and diluted in sterile PBS for a 1mg/ml working solution. *Slco1c1*(BAC)-Cre; *Krit1*$^{fl/fl}$; littermate pups were injected intraperitoneally at P2 with either 50ug of rapamycin (volume of 50 ul) or vehicle and harvested at P10.

For adult rapamycin experiments, either drug or vehicle was administered to adult *Krit1*$^{fl/fl}$; R26-LSL-*Pik3ca*^{H1047R} mice who underwent open craniotomy and injected with AAV-Cre. 50mg of rapamycin powder was dissolved in 1mL 100% ethanol to create a stock solution of which 1mg was freshly prepared in 5% DMSO in sterile PBS for every injection. Intraperitoneal injections of either rapamycin or vehicle (5% DMSO) began on post-operative day 7 when nascent cavernoma lesions could be visualized under microscopy. Injections were performed daily within a two-hour window until animals were harvested on post-operative day 21 at either a low dose (100µg) or high dose (400µg).

For KLF4 BEC-GOF rapamycin experiments, either 100ug of vehicle or rapamycin was injected intraperitoneally (50 µl total volume) to P10 *Slco1c1*(BAC)-Cre; R26-LSL-rtTA;tetOn-KLF4 and littermate *Slco1c1*(BAC)-Cre; R26-LSL-rtTA pups. To induce KLF4 expression, 400 µg of doxycycline was administered via oral gavage. Animals were harvested at P14.

Human CCM Collection

Human CCM tissue specimens were obtained from surgically resected specimens from three sources including the Barrow Neurological Institute, Angioma Alliance biobank, and University of Chicago. This study was approved by each institutions respective Institutional Review Board.

Human Brain AVM Collection

Brain AVM tissue specimens were obtained from the nidal tissue of surgically resected brain AVMs (M.T.L). For non-vascular lesion controls (NVLCs), temporal lobe specimens were similarly acquired from subjects undergoing anterior temporal lobectomies for medically refractory epilepsy. All tissues were frozen at -80 degrees and stored in a biobank. This study was approved by the University of California San Francisco Institutional Review Board and performed in compliance with the Health Insurance Portability and Accountability Act regulations.

DNA Extraction

DNA from human CCM samples was extracted using the DNeasy Blood and Tissue Kit (Qiagen). Extractions were done as per the manufacturers' directions excepting cases where less than 25mg of tissue was available. For samples <25mg the manufacturer recommended volumes were either halved or quartered – depending on the amount of tissue available – to optimize final DNA concentration and yield. Final DNA concentrations were quantified using Qubit dsDNA BR assay kit (Invitrogen cat. Q32850) according to manufacturer recommended protocol.

Droplet Digital PCR

Identification of somatic *PIK3CA* mutations was performed using droplet digital PCR (ddPCR) according to manufacturer protocol for mutation detection assays (BioRad *10047489 Ver B*). For each sample with sufficient DNA yield, 30-100ng of DNA was incorporated into droplets using the QX200 AutoDG system (BioRad). After PCR, fluorescence from the resulting droplets was read using the QX200 droplet reader (Bio-Rad). These steps were repeated for three assays testing the presence of the three most common *PIK3CA* mutations: E542K, E545K, and H1047 (ThermoFisher assay IDs: Hs000000085_rm, Hs000000086_rm, Hs000000088_rm, respectively). Each assay included a no-template control, a wild-type control, and a mutation-positive control for the mutation being assayed. The mutation-positive controls were DNA extracted from cell lines with known heterozygous mutation of E542K (T84), E545K (HCT15), or H1047R (HCT116). The output of the droplet reader was analyzed using the QuantaSoft software (BioRad). The gates for positive and negative mutation status were drawn with respect to the distribution of droplets in the mutation-positive controls and applied to all samples.

SNaPshot

Human CCM samples with an E542K, E545K, or H1047R *PIK3CA* mutation identified by sequencing or ddPCR underwent tertiary confirmation of mutation status using SNaPshot (Applied Biosystems), a single-base extension sanger sequencing assay. An initial round of PCR amplified exons 9 and 20. In a second round of PCR, primers directly adjacent to the assayed nucleotide was extended with ddNTPs and sequenced on a 3130 Genetic Analyzer (Applied Biosystems). Sequences were examined using GeneMapper software (Applied Biosystems). The allele frequency of the mutation by dividing the area under the peak of the mutant allele by the total area under both allele peaks. The primers used in this analysis were synthesized according to designs in a previously published assay for PIK3CA mutations[48].

Sequencing

Previous studies identifying somatic mutations in CCMs and bAVMs have reported alternate allele frequencies less than 1%. To enable the detection of variants at such low frequencies we aimed to sequence samples to an average of 1000x (actual mean coverage 1102x) coverage in addition to leveraging 10bp unique molecular identifiers (UMIs) to mitigate the impact of PCR duplication. These conditions allow us to theoretically detect variants as low as 0.5% allele frequency.

Sequencing libraries for the human CCMs and bAVMs were prepared using the SureSelect XT HS target enrichment workflow (Agilent). The targeting panel used for sequencing the CCMs covers the following genes: *KRIT1,CCM2,PDCD10,PIK3CA,PTEN,AKT1,KRAS,RAF,NRAS,MAP 2K1,RASA1,TEK,GNAQ,GNA11,MAP2K2,PPP2R5D,ACVRL1,ENG,SMAD4, AKT2,AKT3,CCBE1,CDKN1C,FLT1,FLT4,FOXC2,GATA2,GDF2,GJC2,GLMN, KIF11,MTOR,PIK3R2,PTPN14,SOX18,STAMBP,VEGFC,MAP2K4,MAP3K1, MAPK1,JAK1,JAK2,JAK3,KDR,NOTCH1,PDGFRA,PDGFRB,RET,HRAS,TP5 3,MSH2,MYB,MYCN,MYC,ERBB2,EGFR,NTRK2,ODC1,SLC25A21,PTTG1, TSC1,TSC2,EPHB2,TGFBR1,TGFBR2,TGFBR3.*

The bAVM samples were sequenced using a customized Agilent Comprehensive Cancer panel which covers 175 genes including *PIK3CA*. After library preparation, CCM samples were pooled and sequenced across 1 lane of a HiSeq4000 (illumina) with paired-end 150bp reads. bAVM samples were pooled and sequenced across a NovaSeq6000 SP flow cell (illumina) with paired-end 150bp reads.

Sequence Analysis

Sequencing data was processed according to the GATK (Broad Institute) best practices for somatic short variant discovery with slight modifications for "tumor-only" sequencing data. As a secondary method for

variant discovery we developed custom software designed specifically for the detection of somatic mutations in sequencing data from samples with no available normal tissue. This software was implemented as part of Gonomics, an ongoing effort to develop an open-source genomics platform in the Go programming language. Gonomics can be accessed at github.com/vertgenlab/gonomics.

After variant calling the resulting variants were functionally using snpEff. In this process each variant was annotated with: the protein-level consequence of coding mutations: the predicted impact of missense mutations according to SIFT, PolyPhen2, and PROVEAN; membership in several SNP databases including dbSNP, 1000 Genomes project, and ExAC; and membership in the Catalogue of Somatic Mutations in Cancer (COSMIC). We filtered the resulting list of variants using the following inclusion criteria: >100x total coverage; >5 supporting reads; <90% strand specificity; >0.5% alternate allele frequency; <1% population allele frequency according to the above mentioned SNP databases; and membership in the COSMIC database.

Single-Nucleus DNA Sequencing

Frozen human CCM lesion tissue obtained from medically-indicated, surgical resection were prepared for single-nucleus DNA sequencing (snDNA-seq) following a nuclear isolation protocol provided by L. Martelotto[49]. All steps prior to loading on the Tapestri platform were performed in <3 hours. Nuclei were maintained at 4°C throughout the protocol. Frozen tissue was homogenized by Dounce in Nuclei EZ Lysis Buffer (Sigma-Aldrich), briefly washed, filtered through a 70um mesh, stained with DAPI, and filtered through a 35um mesh. The CCM homogenate was sorted using a FACSAriaII (BD) (70um nozzle, 70psi, 4-Way Purity, chiller) gating to retain singlet DAPI-positive events (Extended Data Fig. 7b). Up to 400,000 sorted nuclei were collected in 1ml of the following buffer prepared with ultrapure nuclease-free water: Na_2SO_4 82mM, K_2SO_4 30mM, glucose 10mM, HEPES 10mM, $MgCl_2 \cdot 6H_2O$ 5mM, BSA 2%. Sorted nuclei were pelleted by centrifugation at 4°C (500rcf, 10min), supernatant discarded, and resuspended in 36ul of MissionBio Cell Buffer. The concentration of nuclei was determined by counting DAPI-positive nuclei with a hemocytometer on an EVOS FL (fluorescence) microscope (Thermo Fisher) while confirming that nuclei aggregates comprised <5% of total nuclei. Samples with <5% aggregate nuclei and a concentration within 2000-4000 nuclei/ul (diluting with additional MissionBio Cell Buffer where necessary) were used for snDNA-seq.

Library preparation was performed using the Tapestri platform (MissionBio) according to the manufacturers protocol (PN3354). Libraries were generated with a custom amplicon panel synthesized by MissionBio covering all exons of *KRIT1, CCM2, PDCD10*, and 7 amplicons covering somatic mutation hotspots in *PIK3CA*, per the COSMIC database. Up to three libraries were pooled and sequenced with a NextSeq Mid-Output 2x150bp kit (illumina). Data processing and QC was performed by the MissionBio cloud-based analysis pipeline. Data quality for each nuclei barcode was determined using MissionBio recommended filtering settings. Data from low quality nuclei barcodes were removed prior to mutation analysis. Following these filtering steps, the allele frequency of mutations detected by snDNAseq show high concordance with allele frequencies determined by bulk sequencing (Extended Data Fig. 7c-e).

To determine the cellular phase of somatic mutations detected in bulk sequencing, nuclei barcodes were selected that had a minimum of 20x coverage across all mutant regions to ensure that all nuclei included in the analysis have appropriate sensitivity to detect a mutation (Extended Data Fig. 7c-e). For each nuclei barcode and each mutant position, reads containing the ref and alt alleles were counted and recorded in Supplemental Table 2. Mutant regions that had both a minimum of 10 alt reads and 10% allele frequency were marked as mutation positive. The number of nuclei barcodes with each possible genotype are recorded in Extended Data Fig. 7f.

The p value for each sample was determined by Chi-squared test comparing the observed number of triple mutant nuclei barcodes (or double mutant if only two mutations were identified) to the expected number of triple mutant nuclei barcodes if the null hypothesis is true. In this test the null hypothesis is that the observed somatic mutations do not occur in the same cell and instead exist in two clonal populations where the proportion of each population = 2 • variant allele frequency (assuming cells are diploid and heterozygous for the mutation). In samples where three somatic mutations were identified an alternative null hypothesis may be to use three clonal populations, however assuming that the three somatic mutations are partitioned into two clonal populations as asserted above is a more conservative test and therefore used here. To determine the expected number of triple mutant nuclei barcodes we first determined the expected number of droplets with two (or more) nuclei by approximating a Poisson distribution. The expected number of triple mutant nuclei barcodes is the product of the number of droplets with two nuclei, the proportion of mutant clone 1, and the proportion of mutant clone 2.

Here we report the Poisson estimation p value as this is the accepted method for estimating the rates of false-positive droplets when dealing with data generated using microfluidics. We can also consider a more intuitive upper bound for the p value by considering the extreme case where each droplet contains two nuclei. In this case the expected number of triple mutant nuclei barcodes is the product of the total number of nuclei barcodes, the proportion of mutant clone 1, and the proportion of mutant clone 2. Even in this extreme case the highest p value among our data is <1e-17.

Statistics

All neonatal experimental and control animals were littermates and none were excluded from analysis at the time of harvest. Experimental animals were excluded at the pre-defined point: (i) failure to properly inject the inducing agent (4OHT, tamoxifen, rapamycin) and (ii) observation of significant leakage. Sample sizes were estimated based on our previous experience with the neonatal CCM model and microCT quantification of lesion volume, as previously described[2,5]. All data were analyzed with GraphPad Prism software (version 8) and represented as mean ± SEM. P values were calculated using an unpaired 2-tailed Welch's t-test, or one-way ANOVA and Tukey test for multiple comparisons as indicated in the figure legends. A log-rank test was used to assess the Kaplan-Meier survival curves. P values less than 0.05 were considered statistically significant and are denoted as follows: *<0.05, **<0.01, ***<0.001 and ****<0.0001.

Reporting summary

Further information on research design is available in the Nature Research Reporting Summary linked to this paper.

Materials availability

Transgenic mouse lines not available through public repositories are available from Mark Kahn under a material transfer agreement with the University of Pennsylvania.

Data availability

The data that support the findings of this study are available from the corresponding author upon reasonable request. DNA sequencing data are available on request from DM. The data are not publicly available due to them containing information that could compromise research participant privacy and consent. Public datasets used in this research are available at the following links: COSMIC (cancer.sanger.ac.uk/cosmic), dbSNP (ncbi.nlm.nih.gov/snp), 1000 Genomes Project (internationalgenome.org), ExAC (gnomad.broadinstitute.org) Source data are provided with this paper.

Code availability

Variant calling software was implemented as part of Gonomics, an ongoing effort to develop an open-source genomics platform in the Go programming language. Gonomics can be accessed at github.com/vertgenlab/gonomics.

40. Wang, Y. *et al*. Ephrin-B2 controls VEGF-induced angiogenesis and lymphangiogenesis. *Nature* **465**, 483-486, nature09002 [pii] https://doi.org/10.1038/nature09002 (2010).
41. Ridder, D. A. *et al*. TAK1 in brain endothelial cells mediates fever and lethargy. *J Exp Med* **208**, 2615-2623, https://doi.org/10.1084/jem.20110398 (2011).
42. Claxton, S. *et al*. Efficient, inducible Cre-recombinase activation in vascular endothelium. *Genesis* **46**, 74-80, https://doi.org/10.1002/dvg.20367 (2008).
43. Chan, A. C. *et al*. Mutations in 2 distinct genetic pathways result in cerebral cavernous malformations in mice. *J Clin Invest* **121**, 1871-1881, 44393 [pii] https://doi.org/10.1172/JCI44393 (2011).
44. Foster, K. W. *et al*. Induction of KLF4 in basal keratinocytes blocks the proliferation-differentiation switch and initiates squamous epithelial dysplasia. *Oncogene* **24**, 1491-1500, https://doi.org/10.1038/sj.onc.1208307 (2005).
45. Trotman, L. C. *et al*. Pten dose dictates cancer progression in the prostate. *PLoS Biol* **1**, E59, https://doi.org/10.1371/journal.pbio.0000059 (2003).
46. Adams, J. R. *et al*. Cooperation between Pik3ca and p53 mutations in mouse mammary tumor formation. *Cancer Res* **71**, 2706-2717, https://doi.org/10.1158/0008-5472.CAN-10-0738 (2011).
47. Korbelin, J. *et al*. A brain microvasculature endothelial cell-specific viral vector with the potential to treat neurovascular and neurological diseases. *EMBO Mol Med* **8**, 609-625, https://doi.org/10.15252/emmm.201506078 (2016).
48. Hurst, C. D., Zuiverloon, T. C., Hafner, C., Zwarthoff, E. C. & Knowles, M. A. A SNaPshot assay for the rapid and simple detection of four common hotspot codon mutations in the PIK3CA gene. *BMC Res Notes* **2**, 66, https://doi.org/10.1186/1756-0500-2-66 (2009).
49. Martelotto, L. G. 'Frankenstein' protocol for nuclei isolation from fresh and frozen tissue for snRNAseq. *protocols.io* https://doi.org/10.17504/protocols.io.3fkgjkw (2020).

Acknowledgements We thank the members of the Kahn lab for their thoughtful comments and advice during this work. We thank Angioma Alliance for patient enrollment, and the University of Chicago PaleoCT core facility for its expertise in imaging and image quantitation. We thank the Penn CDB Microscopy Core for support with microscopy. Flow cytometry was performed in the Duke Human Vaccine Institute Research Flow Cytometry Shared Resource Facility. We thank Duke University School of Medicine for use of the Sequencing and Genomic Technologies Shared Resource for library preparation and sequencing. These studies were supported by National Institute of Health grants R01HL094326 and R01NS100949 (MK), P01NS092521 (MK, DM, IA) the Leducq Foundation (MK, MP), the AHA-Allen foundation (MK), T32 HL007150 (AR), F31HL152738 (DS), F31NS115256 (CH), F30NS100252 (AT), European Research Council (ERC) Synergy Grant-2019-WATCH-810331 (MS) and ERC Consolidator Grant EMERGE-773047 (MP).

Author contributions AAR designed and performed most of the mouse and tissue culture experiments and wrote the manuscript. DAS performed the genetic studies of human CCM lesions and wrote the manuscript. SYS created and performed the adult cranial window assays in mice. CCH, ATT and MRD contributed to mouse genetic studies. MC performed in vitro studies. NH, RG, SR, RL, TM, RS and IAA performed microCT CCM lesion imaging and quantification in a blinded manner. MC and PM assisted with mouse genetic studies. JY and DCS performed histologic studies. MTL provided surgically excised human CCM samples. MS and JK provided critical reagents. MP, IAA, DAM and MK designed experiments and wrote the manuscript.

Competing interests IAA is Chairman of the Scientific Advisory Board for Angioma Alliance and provides expert opinions related to clinical care of cerebral cavernous malformations. All other authors declare no competing interests.

Additional information

Supplementary information The online version contains supplementary material available at https://doi.org/10.1038/s41586-021-03562-8.

Correspondence and requests for materials should be addressed to D.A.M. or M.L.K.

Peer review information *Nature* thanks Marcus Goncalves, Mustafa Sahin, Salim Seyfried and the other, anonymous, reviewer(s) for their contribution to the peer review of this work. Peer review reports are available.

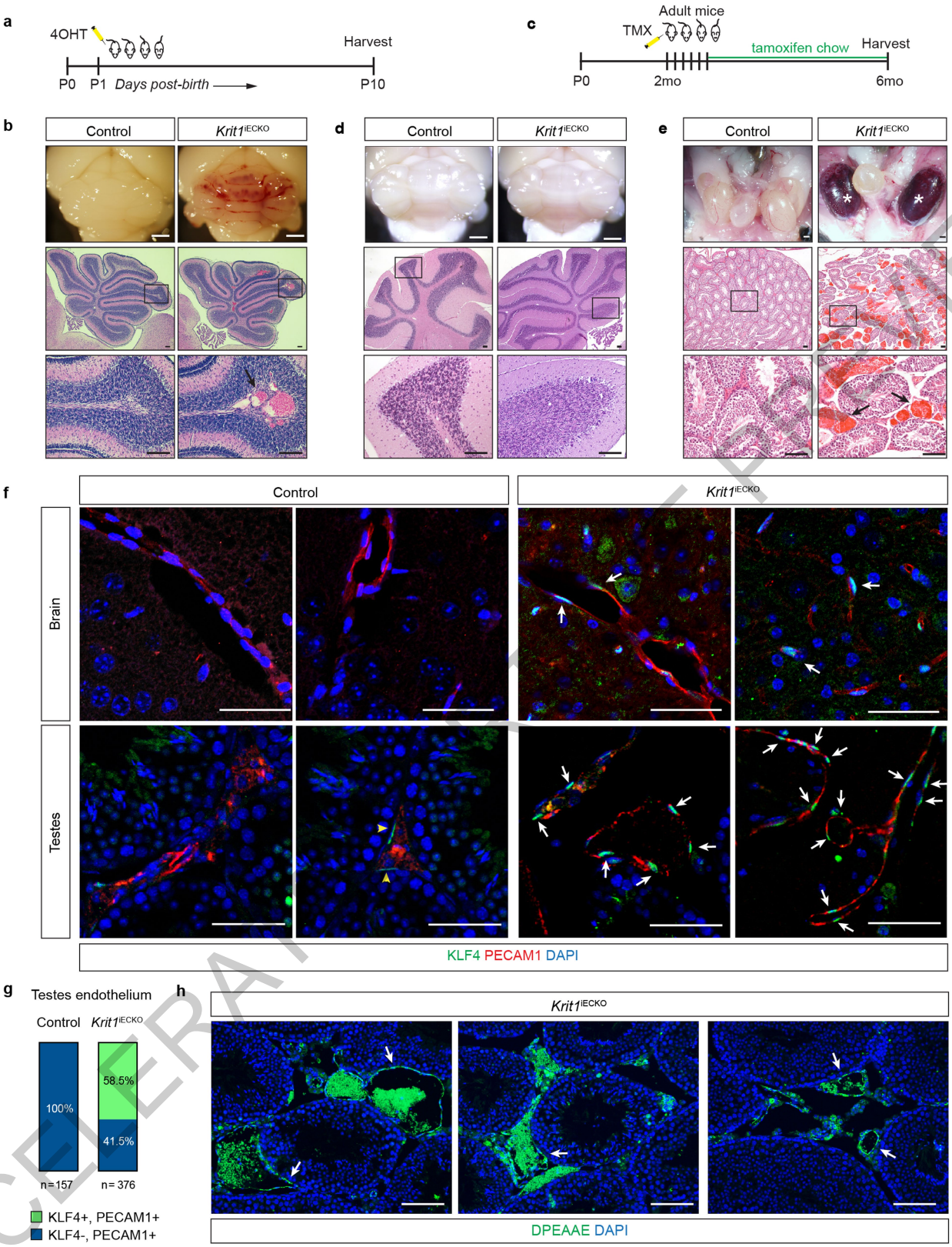

Extended Data Fig. 1 | See next page for caption.

Extended Data Fig. 1 | Endothelial loss of CCM function in adult mice confers cavernous vascular malformations in the testis but not the brain. **a**, Schematic of the neonatal endothelial CCM deletion experiment. **b**, Cavernous malformations form by P10 in the hindbrain of *Krit1*^{iECKO} animals with a susceptible gut microbiome. Images of hindbrains from the indicated animals are shown above, and Hematoxylin-Eosin (H-E) stained histologic sections shown below. Arrow indicates a CCM lesion in the white matter venous vessel. **c**, Schematic of CCM gene deletion in endothelial cells (ECs) of adult mice on a susceptible microbiome background. **d**, Cavernous malformations are not detected in the brain of 6 month old *Krit1*^{iECKO} animals following tamoxifen administration. Images of hindbrains from the indicated animals are shown above, and H-E stained histologic sections shown below. **e**, Cavernous malformations are detected in the testis of 6 month old *Krit1*^{iECKO} animals. Images of testis from the indicated animals are shown above and H-E stained histologic sections shown below. * indicate blood-filled testes. Arrows indicate cavernous blood-filled vessels around the seminiferous tubules. For panels **b, d, e:** Visual images representative of *n*=4 animals/genotype; H-E histology representative of 6 tissue sections from *n*=4 animals. Scale bars for visual images, 1mm; scale bars for histology, 0.1mm. **f**, Immunostaining for KLF4 and endothelial cell marker PECAM1 in brain (top) and testis (bottom) from the experiment in **c** is shown. Note endothelial CCM LOF in adult mice results in KLF4 upregulation without CCM formation in the brain. Arrows indicate KLF4+ nuclei in PECAM1+ ECs. Yellow arrowheads indicate KLF4+ peritubular myoid cells. Scale bars, 50 microns. **g**, Quantitation of KLF4+ and KLF4- ECs identified using co-staining for KLF4 and PECAM1 in testis is shown. Quantitation from 10 individual 800micron x 800micron HPF from 3 individual animals. **h**, Immunostaining for DPEAAE, a versican neo-epitope exposed by ADAMTS-mediated proteolysis, is shown for *Krit1*^{iECKO} testis. Arrows indicate peri-endothelial cell detection of DPEAAE around testicular cavernomas. Scale bars, 0.1mm. "Control" genotype in panels **b, d, e, f, g** indicate animals with genotypes of either *Cdh5*-CreERT2; *Krit1*$^{fl/+}$ or *Krit1*$^{fl/fl}$. Immunofluorescence images in **f & h** representative of 6 tissue sections from *n*=4 individual animals/genotype.

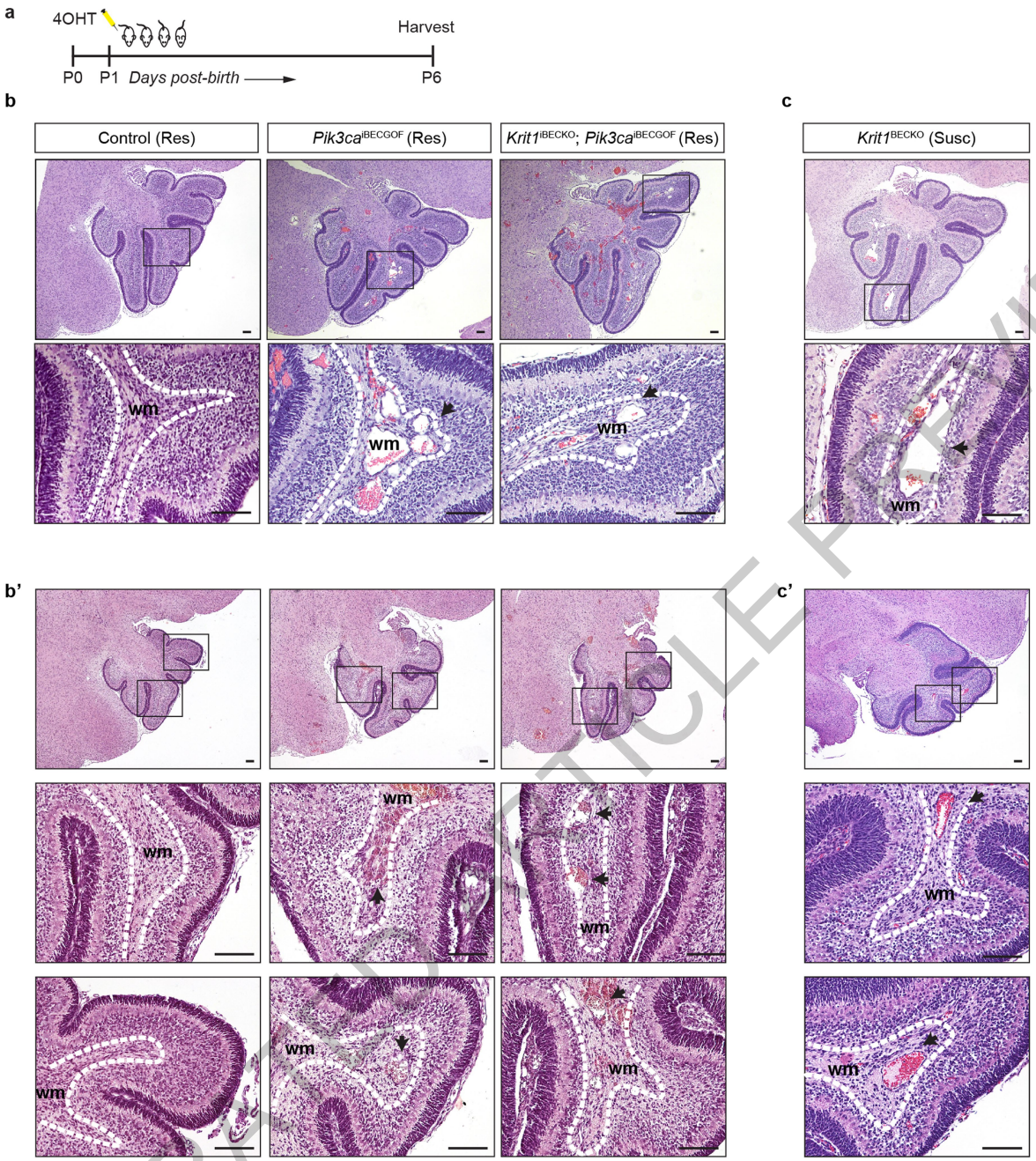

Extended Data Fig. 2 | Vascular lesions due to CCM LOF and/or PIK3CA GOF arise in veins of the white matter. a, Schematic of neonatal endothelial induction of *Krit1* deletion and/or PIK3CA^{H1047R} expression. **b & c**, Hematoxylin-Eosin (H-E) staining of saggital hindbrain sections from P6 control, *Pik3ca*^{iBECGOF}, *Krit1*^{iBECKO}; *Pik3ca*^{iBECGOF} (**b** and **b'**) and *Krit1*^{iBECKO} (**c** and **c'**) animals with a resistant (Res) or susceptible (Susc) microbiome. **b'** and **c'** samples were obtained from animals distinct from those in **b** and **c**. Note that lesions form in the white matter with both CCM loss of function and PIK3CA gain of function. Boxes in upper images denote area of magnified image immediately below. Dotted lines outline the white matter of the cerebellum. Arrows indicate lesions in white matter veins and venules. H-E images representative of 6 tissue sections from *n*=4 animals/genotype. wm, white matter. Scale bars, 0.1mm.

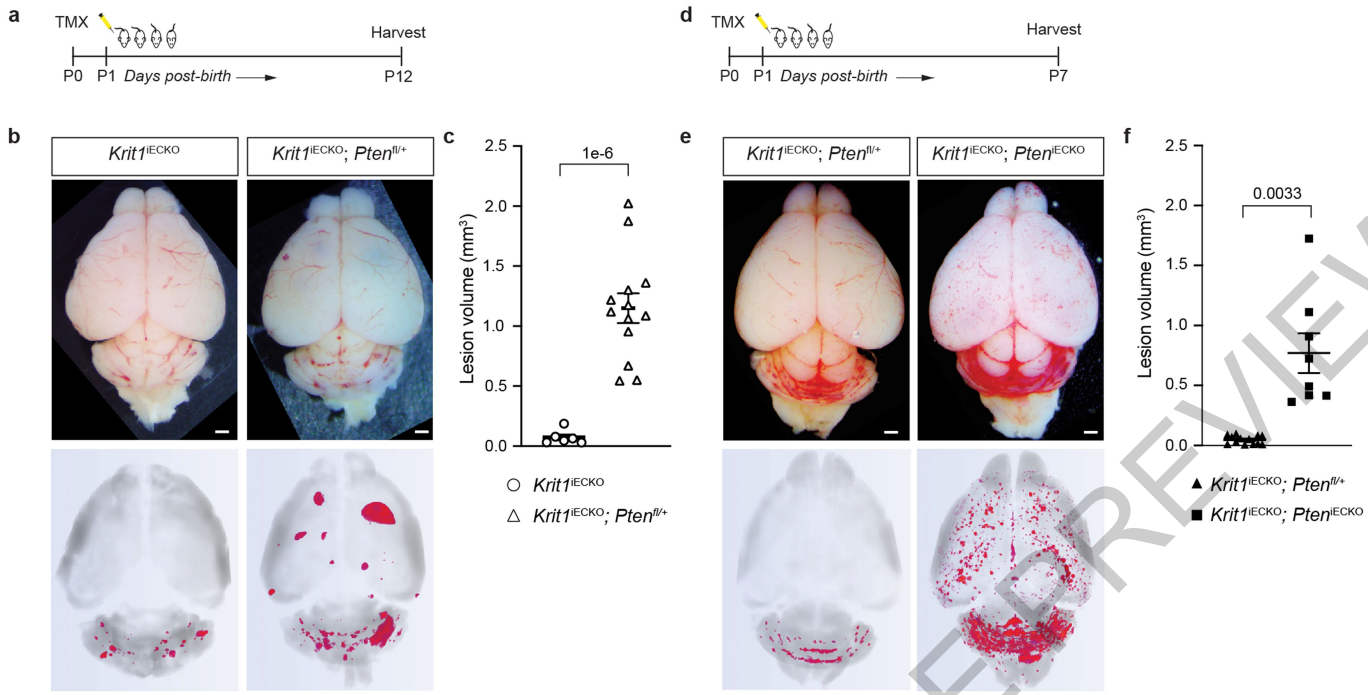

Extended Data Fig. 3 | Endothelial *Pten* LOF synergizes with *Krit1* LOF in a dose-dependent manner. a, Schematic of neonatal endothelial induction with tamoxifen of *Krit1* deletion and deletion of either none or one allele of *Pten* in endothelial cells using a *Pdgfb*-CreERT2 transgene. **b**, Representative visual and paired microCT images of *Krit1*^{iECKO} and *Krit1*^{iECKO};*Pten*$^{fl/+}$ littermate mice on a susceptible microbiome background at P12. Scale bars, 1mm. These mice were produced from a *Pten*$^{fl/+}$ x *Pten*$^{fl/+}$ cross; however no *Krit1*^{iECKO};*Pten*$^{fl/fl}$ littermates survived to P12. **c**, MicroCT quantification of lesion volumes at P12. (*Krit1*^{iECKO}, *n*=6; *Krit1*^{iECKO};*Pten*$^{fl/+}$, *n*=13). **d**, Schematic of neonatal endothelial induction of *Krit1* deletion and deletion of either one or both alleles of *Pten* in endothelial cells using a *Pdgfb*-CreERT2 transgene with brains harvested at P7. These mice were produced from a *Pten*$^{fl/+}$ x *Pten*$^{fl/fl}$ cross. **e**, Representative visual and paired microCT images in *Krit1*^{iECKO};*Pten*$^{fl/+}$ and *Krit1*^{iECKO};*Pten*^{iECKO} littermate mice at P7. Scale bars, 1mm. **f**, MicroCT quantification of lesion volumes at P7. (*Krit1*^{iECKO};*Pten*$^{fl/+}$, *n*=13; *Krit1*^{iECKO};*Pten*^{iECKO}, *n*=8). Data are mean ± s.e.m. Unpaired, two-tailed Welch's t-test.

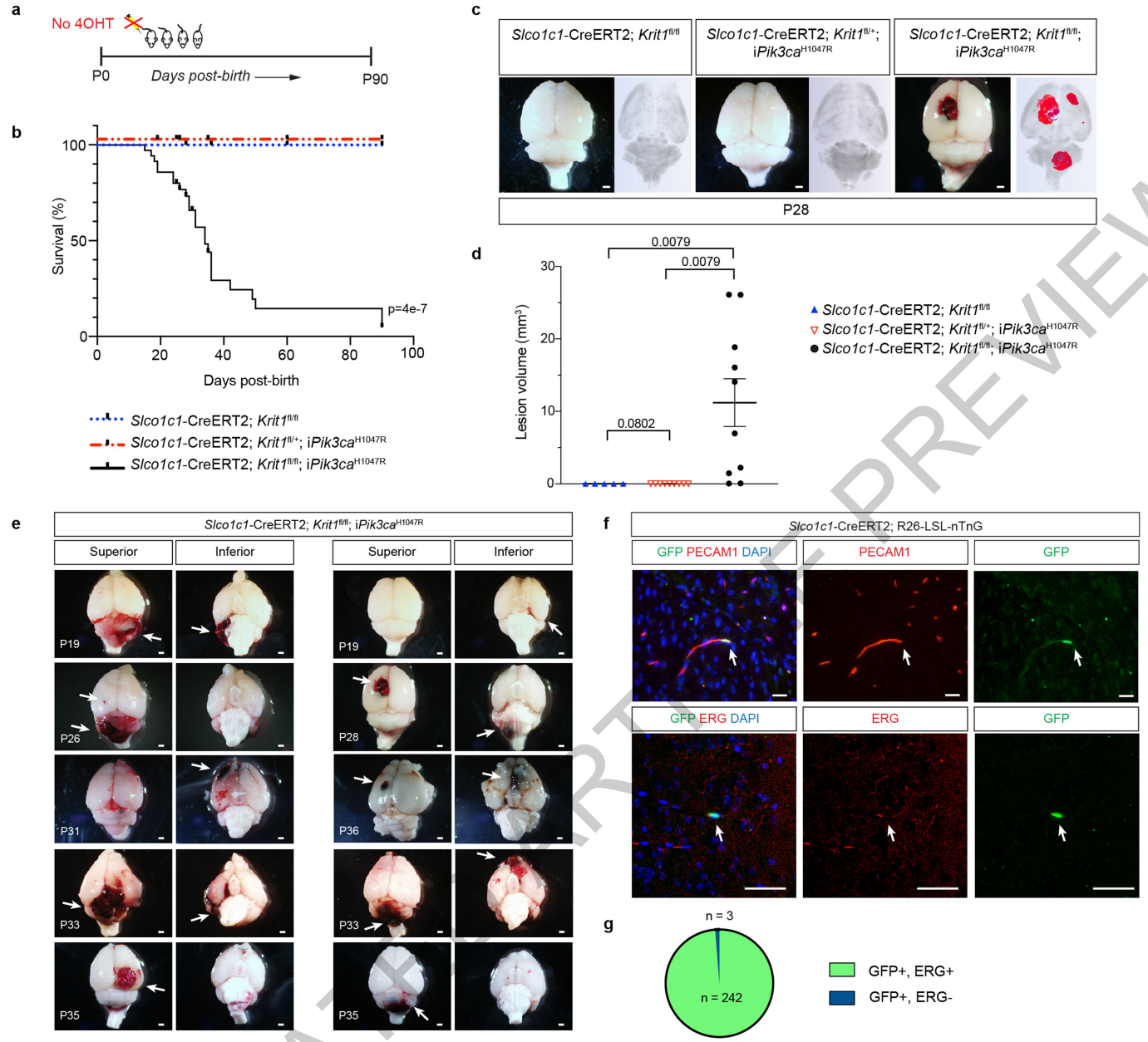

Extended Data Fig. 4 | Uninduced *Slco1c1*-CreERT2; *Krit1*$^{fl/fl}$; i*Pik3ca*^{H1047R} animals develop focal lesions due to *Slco1c1*-CreERT2 transgene endothelial leak. a, Schematic for generation of a survival curve in the absence of tamoxifen administration. **b**, Postnatal survival curve in the absence of tamoxifen administration is shown for indicated genotypes. (*Slco1c1*-CreERT2;*Krit1*$^{fl/fl}$, *n*=15, *Slco1c1*-CreERT2;*Krit1*$^{fl/+}$;i*Pik3ca*^{H1047R} *n*=10, *Slco1c1*-CreERT2;*Krit1*$^{fl/fl}$;i*Pik3ca*^{H1047R} *n*=39). Log-rank test. **c**, Representative visual and paired microCT images of brains harvested from untreated P28 littermates. Scale bars, 1mm. **d**, MicroCT quantitation of lesion volumes of untreated P28 animals. (*Slco1c1*-CreERT2; *Krit1*$^{fl/fl}$, *n*=5, *Slco1c1*-CreERT2;*Krit1*$^{fl/+}$;i*Pik3ca*^{H1047R} *n*=9, *Slco1c1*-CreERT2;*Krit1*$^{fl/fl}$; i*Pik3ca*^{H1047R} *n*=10). Data are mean ± s.e.m. Unpaired, two-tailed Welch's t-test. **e**, Additional visual images of brains from a superior and inferior perspective from animals harvested at various timepoints (P19-P36). Arrows point to focal vascular lesions. Scale bars, 1mm. **f**, Leak assessed by immunostaining of brain sections with antibodies against GFP to identify Cre-expressing cells, and cell surface marker PECAM1 (top) and nuclear protein ERG (bottom) to identify endothelial cells is shown. Scale bars, 50 microns. Immunofluorescence images representative of 10 tissue sections from *n*=4 individual animals/genotype. **g**, Quantitation of GFP+; ERG+ nuclei (n = 242) and GFP+; ERG- nuclei (n = 3) from 20 individual 800micron x 800micron HPF.

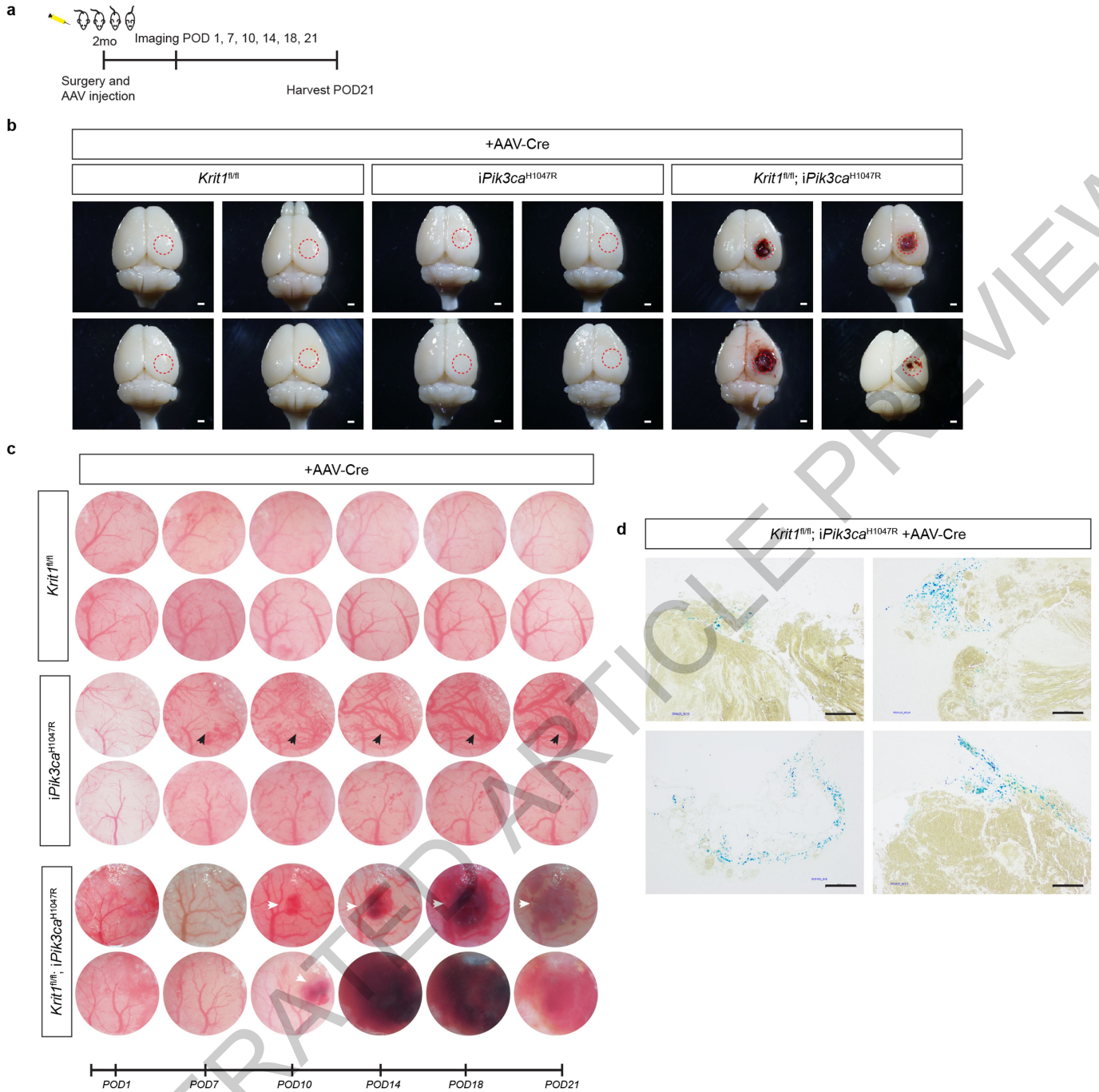

Extended Data Fig. 5 | Exogenous delivery of Cre recombinase via AAV vector to drive combined loss of CCM function and gain of PIK3CA function results in CCM formation in the adult brain. a, A schematic of the experimental approach in which a cranial window is created and AAV-Cre virus injected into the brains of 2 month old mice with serial imaging at post-operative days 1, 7, 10, 14, 18, and 21. **b**, Representative visual images of brains harvested 21 days after injection of AAV-Cre into adult animals. Dotted circles indicate the site of cranial window and AAV-Cre injection. Includes visual images displayed in Figure 1. Scale bars, 1mm. **c**, Serial images obtained through the same cranial window of mice of indicated genotypes following injection of AAV-Cre. i*Pik3ca*^{H1047R} designation includes i*Pik3ca*^{H1047R} and/or *Krit1*$^{fl/+}$;i*Pik3ca*^{H1047R} genotypes. White arrows indicate cavernous malformations in *Krit1*$^{fl/fl}$;i*Pik3ca*^{H1047R} mice. Black arrows indicate hypervascularity in i*Pik3ca*^{H1047R} mice. **d**, Peri-lesional iron deposition stain in brains indicative of chronic bleed from four independent *Krit1*$^{fl/fl}$;i*Pik3ca*^{H1047R} mice at post-op day 21. Scale bars, 200 microns.

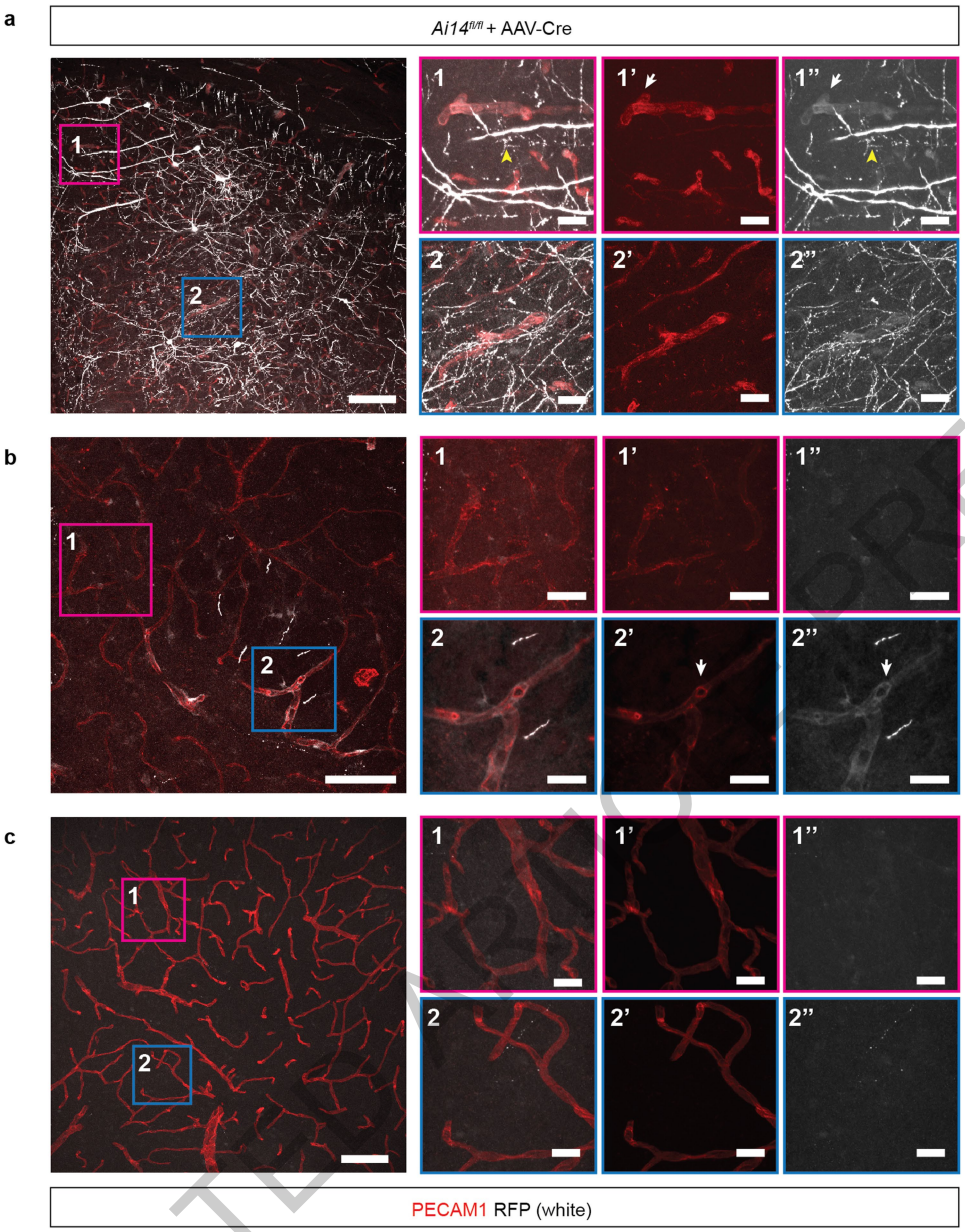

Extended Data Fig. 6 | Lineage tracing of AAV-Cre activity after direct injection into the mouse brain. AAV-Cre virus was injected into the brain of Ai14 Cre reporter animals and Cre activity assessed by detection of the tdTomato (RFP) reporter 14 days after injection. **a-c**, Confocal microscopic overview from **a**, the injection site; **b**, the border region of the viral spread and **c**, the contralateral cortex of AAV-Cre injected Ai14 mice two weeks after stereotactic injection. AAV-Cre transduced cells expressed red fluorescent protein (RFP) (shown in white). RFP-positive vessels were identified by colocalization with PECAM1 (shown in red). White arrows point to representative RFP-positive vessels. Yellow arrowheads point to RFP-expressing neuronal cells. Scale bar, 100 microns. Boxed regions in 1 and 2 are shown at higher magnification on the right. 1 & 2 show PECAM1 staining for endothelial cells overlaid with RFP signal; 1′ & 2′ show PECAM staining alone; 1″ & 2″ shown RFP staining alone. These data are representative 12 separate images from 8 tissue sections from n=2 individual animals. Scale bar, 20 microns.

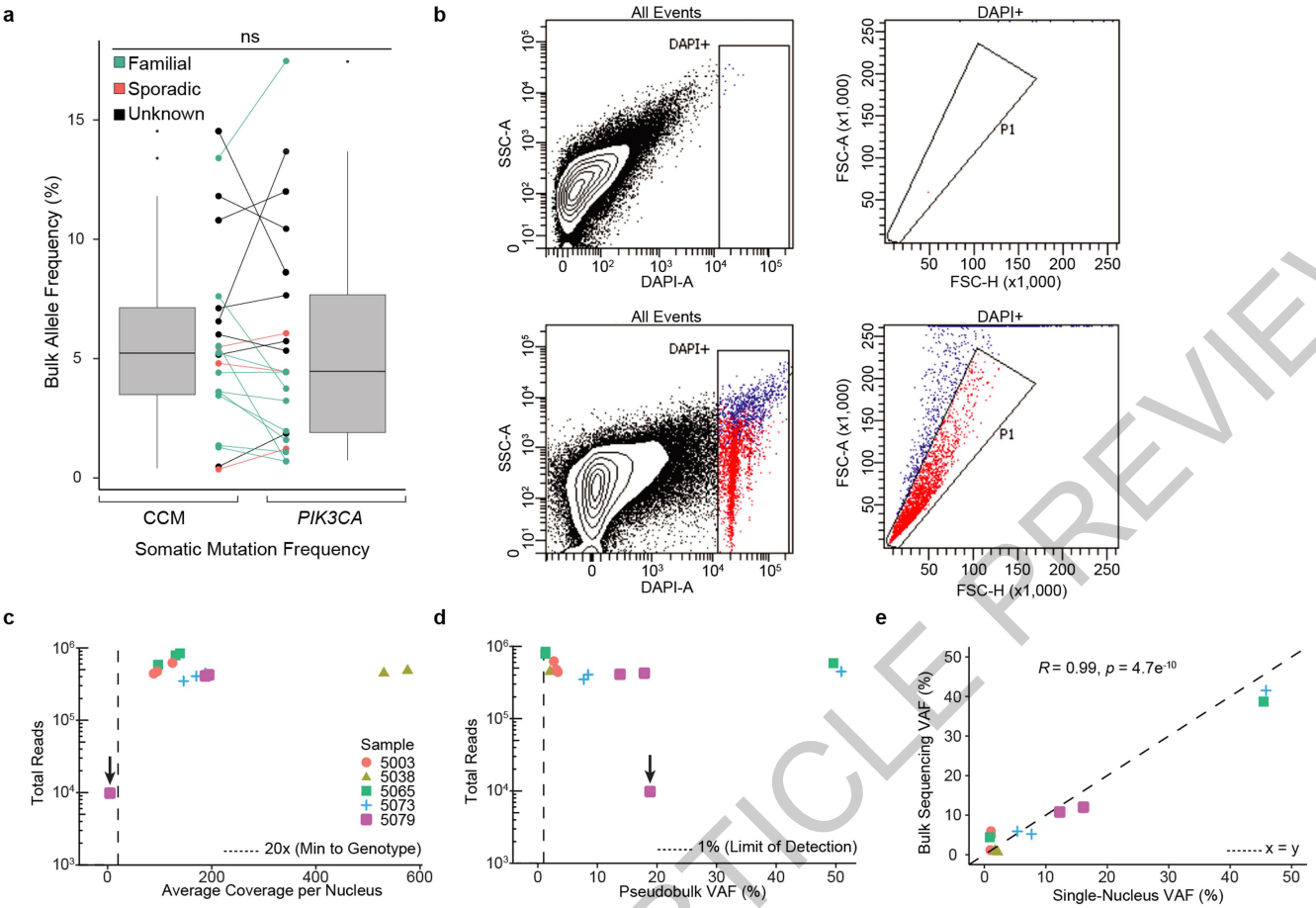

f

Sample	Disease Type	Total Nuclei	*PIK3CA* / CCM Mutation 1 / CCM Mutation 2								p
			+/+/+	*/*/*	*/*/+	*/+/*	+/*/*	*/+/+	+/*/+	+/+/*	
5003	Sporadic	4983	4844	73	6	8	11	19	6	16	2.59E-16
5038	Sporadic	877	834	NA	25	NA	NA	13	5	NA	6.22E-19
5079	Sporadic	2182	1335	NA	391	NA	NA	312	144	NA	7.42E-39
5065	Familial	6040	536	79	17	8	14	2	5378	6	1.90E-18
5073	Familial	2383	165	181	50	20	156	5	1797	9	5.39E-29

Extended Data Fig. 7 | Characterization of single-nucleus DNA sequencing of human CCM samples. a, The relationship between somatic *PIK3CA* and CCM mutations detected in bulk sequencing is graphed. Points indicate individual mutations in either a CCM gene or PIK3CA. Lines connect the CCM gene and PIK3CA gene mutations present in a single sample. Box plots show the aggregate frequencies of *PIK3CA* and CCM mutations. Center lines show the medians; box limits indicate the 25th and 75th percentiles; whiskers extend 1.5 times the interquartile range from the 25th to 75th percentiles, outliers are represented by dots. n = 21 sample points for both plots. **b**, Representative FANS plots of unstained (top row) and DAPI stained (bottom row) CCM homogenate. Doublet discrimination by forward scatter profile for DAPI stained sample. Plots consist of 100,000 events. The unstained sample contains 1 event (0%) in the DAPI+ singlet gate. The DAPI stained samples contains 2,414 events (2.4%) in the DAPI+ singlet gate. **c**, Total reads and average coverage per nucleus from snDNAseq for each mutation detected by bulk sequencing. Dotted line shows 20x coverage, the minimum cutoff used for establishing genotype. **d**, Pseudobulk allele frequency from snDNA-seq for each mutation detected by bulk sequencing. Dotted line shows 1% allele frequency. Note the data point with the arrow in **c**-**d** shows a mutation in sample 5079 detected in bulk sequencing which, due to poor amplification during snDNA-seq, received insufficient coverage per nucleus (4.5x) to establish nuclear genotypes however is clearly present in pseudobulk reads (1849/9814). **e**, Comparison of mutation allele frequency as detected by bulk and snDNA-seq. As nuclei are diploid for the relevant autosomes, the x-axis is equal to the fraction of mutant nuclei divided by two. Dotted line shows perfect correlation at x=y. *R* and *p* were calculated by Pearson's correlation coefficient. **f**, A summary of snDNA-seq results for 3 sporadic and 2 familial CCMs analyzed is shown. The number of nuclei with each possible genotype are listed. + indicates a wild-type allele; * indicates a mutant allele. Note that only 1 somatic CCM mutation was identified in samples 5038 and 5079. P values were determined by two-tailed chi-squared test between the observed and expected triple mutant nuclei (or double mutant for lesions 5038 and 5079) determined by Poisson distribution (see Methods).

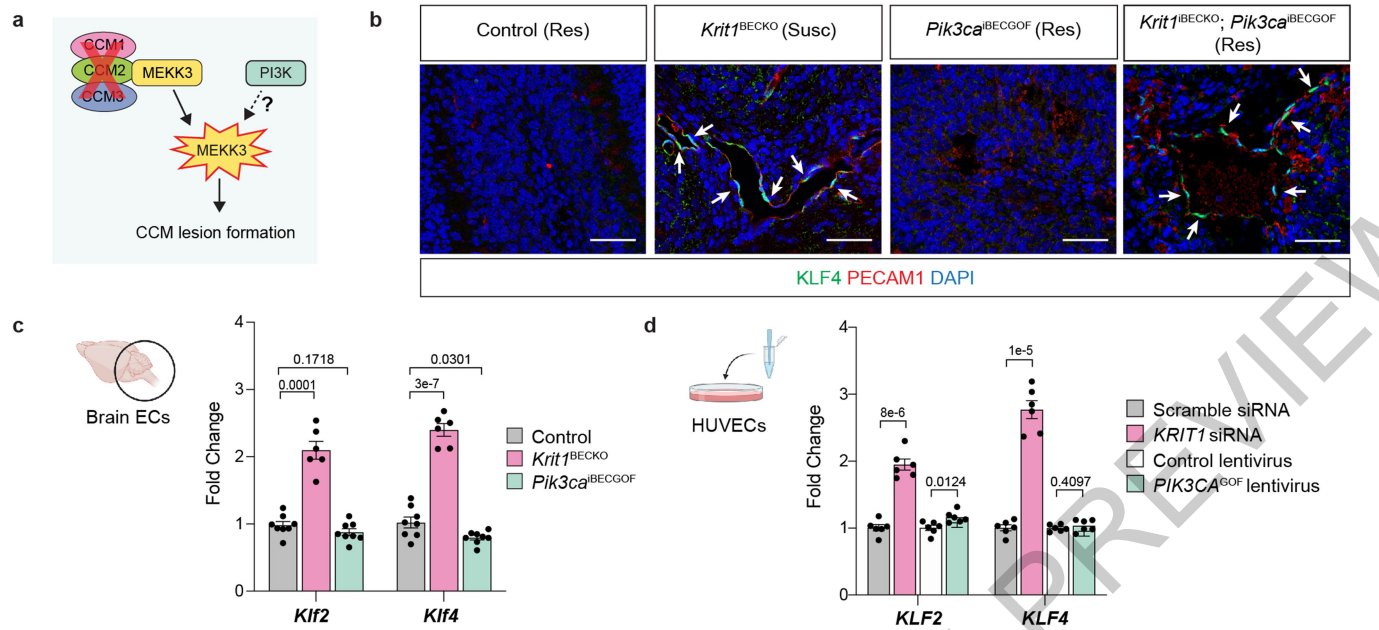

Extended Data Fig. 8 | PI3K signaling does not augment MEKK3-KLF2/4 signaling. a, Diagram of how gain of PI3K signaling might augment CCM formation by acting upstream of MEKK3-KLF2/4 signaling in endothelial cells. **b**, Immunostaining for KLF4 and the endothelial cell marker PECAM1 in hindbrain sections from P6 control, *Krit1*^{BECKO}, *Pik3ca*^{iBECGOF}, and *Krit1*^{iBECKO}; *Pik3ca*^{iBECGOF} neonates with either a susceptible (Susc) or resistant (Res) gut microbiome is shown. White arrows indicate endothelial cell nuclear KLF4 staining. Immunofluorescence images representative of 10 tissue sections from n=4 individual animals/genotype. Control animals are either *Slco1c1*-Cre;*Krit1*$^{fl/+}$ or *Krit1*$^{fl/fl}$. Scale bars, 50 microns. **c**, Measurement of *Klf2* and *Klf4* mRNA in endothelial cells isolated from the hindbrains of P6 control, *Krit1*^{BECKO} and *Pik3ca*^{iBECGOF} neonates. (Control, n=8; *Krit1*^{BECKO}, n=6; *Pik3ca*^{iBECGOF}, n=8). **d**, Measurement of *KLF2* and *KLF4* mRNA in human umbilical vein endothelial cells (HUVECs) treated with the indicated siRNAs or lentiviral vectors. (n=6 individual wells/group over 2 independent experiments). Data are mean ± s.e.m. Unpaired, two-tailed Welch's t-test.

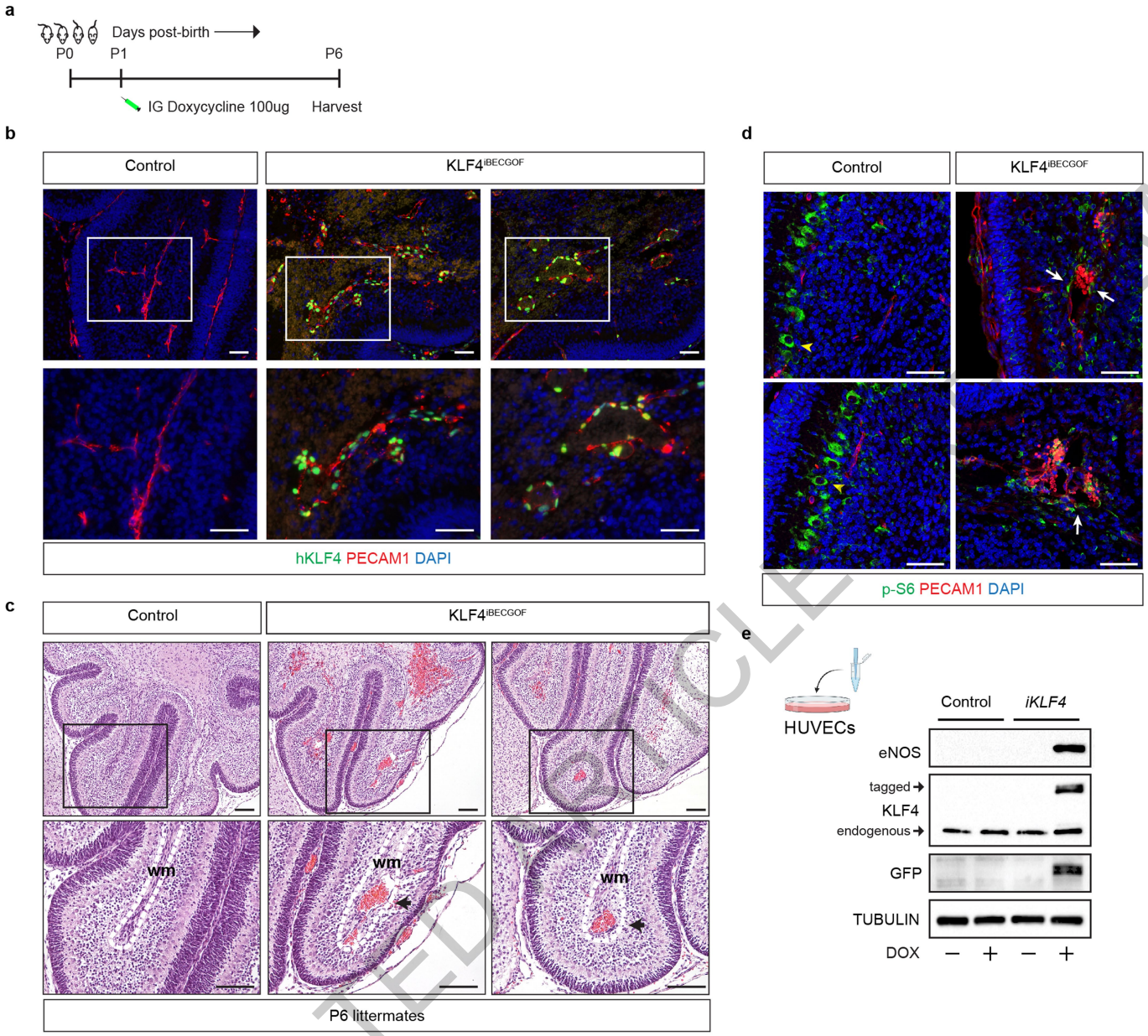

Extended Data Fig. 9 | The CCM effector KLF4 augments endothelial cell PI3K-mTORC1 signaling. a, Schematic of neonatal endothelial induction of KLF4 expression in KLF4^{iBECGOF} animals. **b**, Immunostaining for KLF4 and the endothelial cell marker PECAM1 in hindbrain sections from P6 control and KLF4^{iBECGOF} animals is shown. Boxes in upper images denote area of magnified image immediately below. Immunofluorescence images representative of 6 tissue sections from *n*=4 individual animals/genotype. Scale bars, 50 microns. **c**, H-E stained sections of hindbrain from control and KLF4^{iBECGOF} littermates. Boxes in upper images denote area of magnified image immediately below. Black arrows indicate lesions. Dotted lines outline the white matter of the cerebellum. wm, white matter. Note the dilated white matter venules similar to those observed with CCM loss of function and PIK3CA gain of function shown in Extended Data Figure 2. H-E histology representative of 6 tissue sections from n=4 animals/genotype. Scale bars, 0.1mm. **d**, Immunostaining for phospho-S6 ribosomal protein (p-S6) and the endothelial cell marker PECAM1 in hindbrain sections from P6 control and KLF4^{iBECGOF} animals is shown. White arrows indicate p-S6 positive endothelial cells. Yellow arrowheads into non-endothelial p-S6 positive cells. Immunofluorescence images representative of 6 tissue sections from *n*=4 individual animals/genotype. Scale bars, 50 microns. **e**, Immunoblot detection of KLF4, KLF4-GFP, the KLF4 target gene eNOS in HUVECs without and with inducible lentiviral expression of KLF4-GFP ("i*KLF4*" cells) or control lentivirus. TUBULIN is shown as a loading control.

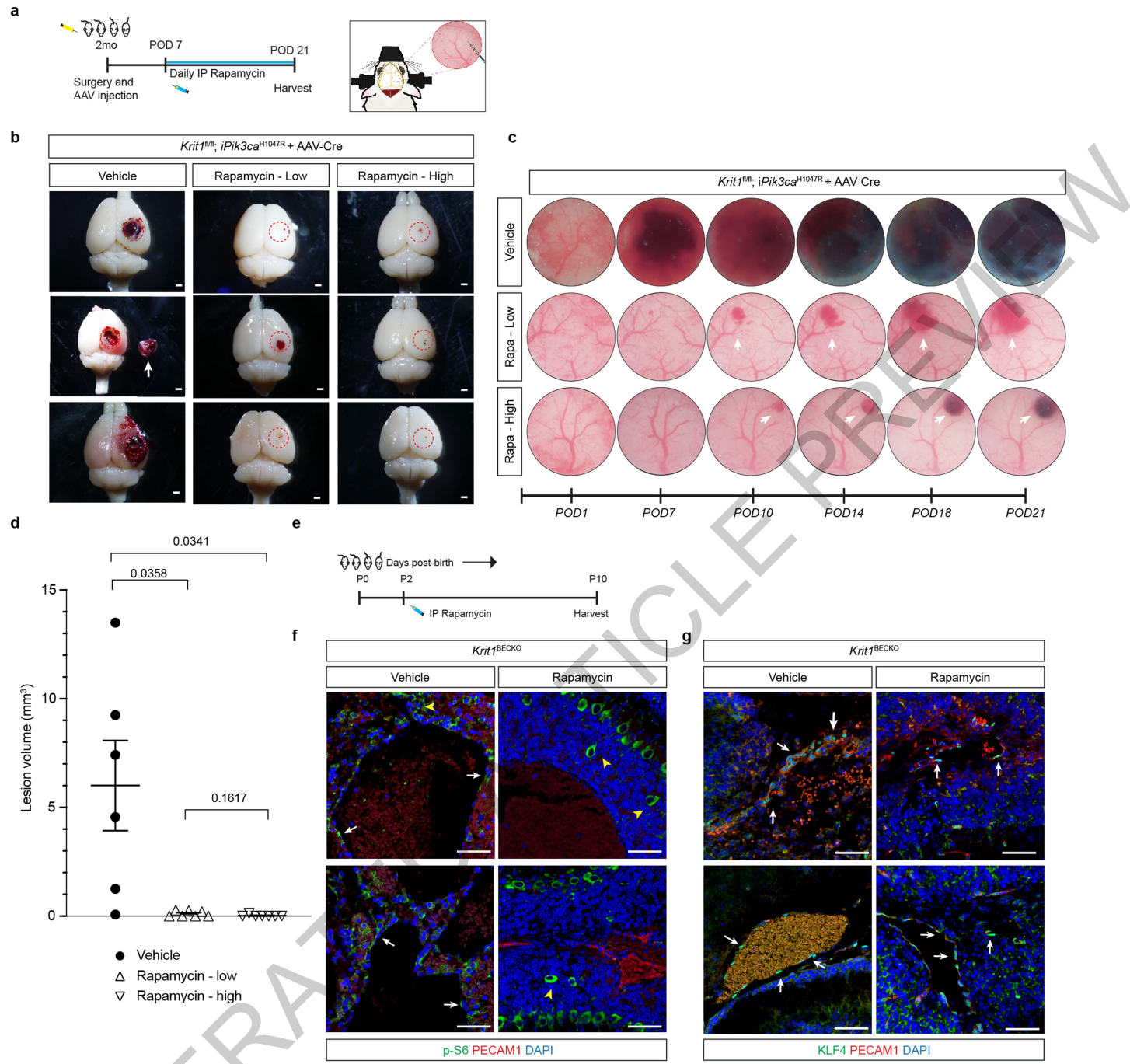

Extended Data Fig. 10 | Rapamycin rescue of CCM formation is independent of KLF4. a, A schematic of the experimental approach in which a cranial window is created and AAV-Cre virus injected into the brains of 2 month old mice and along with daily injection of vehicle, 100ug of Rapamycin (Rapa-low), or 400ug of Rapamycin (Rapa-high) started at post-op day 7 continuing through post-op day 21 with serial imaging at post-op day 1, 7, 10, 14, 18, and 21. **b**, Representative visual images of brains harvested 21 days after injection of AAV-Cre and 2 weeks of daily vehicle or rapamycin (low dose/high dose) treatment in *Krit1*$^{fl/fl}$;*iPik3ca*^{H1047R} mice. Dotted circles indicate the site of cranial window and AAV-Cre injection. Arrows indicate detached lesions. Scale bars, 1mm. **c**, Serial images obtained through the same cranial window of *Krit1*$^{fl/fl}$;*iPik3ca*^{H1047R} mice following injection of AAV-Cre and subsequent treatment. Arrows indicate formation and growth of individual cavernous malformations. **d**, MicroCT quantitation of lesion volumes 21 days after creation of the cranial window and injection of AAV-Cre. Values include duplication of microCT values in Figure 4 (vehicle and low dose treatments). (Vehicle, n=6; Rapa-low, n=7; Rapa-high, n=7). Data are mean ± s.e.m. Unpaired, two-tailed Welch's t-test. **e**, Schematic of neonatal endothelial induction of *Krit1* deletion and treatment with Rapamyin or vehicle control at P2. **f**, Immunostaining of hindbrain sections from P6 *Krit1*^{iBECKO} animals treated with vehicle or Rapamycin for PECAM1 and p-S6. White arrows indicate p-S6 positive endothelial cells in the control but not the Rapmycin treated animal. Yellow arrowheads indicate p-S6 positive neuronal cells. **g**, Immunostaining of hindbrain sections from P6 *Krit1*^{iBECKO} animals treated with vehicle or Rapamycin for PECAM1 and KLF4. White arrows indicate KLF4-positive endothelial cells detected in the control and in the Rapmycin treated animal. Scale bars, 50 microns.

nature research

Corresponding author(s): Mark Kahn, Douglas Marchuk

Last updated by author(s): Jan 5, 2021

Reporting Summary

Nature Research wishes to improve the reproducibility of the work that we publish. This form provides structure for consistency and transparency in reporting. For further information on Nature Research policies, see our Editorial Policies and the Editorial Policy Checklist.

Statistics

For all statistical analyses, confirm that the following items are present in the figure legend, table legend, main text, or Methods section.

n/a	Confirmed
☐	☒ The exact sample size (*n*) for each experimental group/condition, given as a discrete number and unit of measurement
☐	☒ A statement on whether measurements were taken from distinct samples or whether the same sample was measured repeatedly
☐	☒ The statistical test(s) used AND whether they are one- or two-sided *Only common tests should be described solely by name; describe more complex techniques in the Methods section.*
☐	☒ A description of all covariates tested
☐	☒ A description of any assumptions or corrections, such as tests of normality and adjustment for multiple comparisons
☐	☒ A full description of the statistical parameters including central tendency (e.g. means) or other basic estimates (e.g. regression coefficient) AND variation (e.g. standard deviation) or associated estimates of uncertainty (e.g. confidence intervals)
☐	☒ For null hypothesis testing, the test statistic (e.g. *F*, *t*, *r*) with confidence intervals, effect sizes, degrees of freedom and *P* value noted *Give P values as exact values whenever suitable.*
☒	☐ For Bayesian analysis, information on the choice of priors and Markov chain Monte Carlo settings
☒	☐ For hierarchical and complex designs, identification of the appropriate level for tests and full reporting of outcomes
☒	☐ Estimates of effect sizes (e.g. Cohen's *d*, Pearson's *r*), indicating how they were calculated

Our web collection on statistics for biologists contains articles on many of the points above.

Software and code

Policy information about availability of computer code

Data collection	For bulk sequencing: Sequencing libraries for the human CCMs and bAVMs were prepared using the SureSelect XT HS target enrichment workflow (Agilent). The bAVM samples were sequenced using a customized Agilent Comprehensive Cancer panel which covers 175 genes including PIK3CA. After library preparation, CCM samples were pooled and sequenced across 1 lane of a HiSeq4000 (illumina) with paired-end 150bp reads. bAVM samples were pooled and sequenced across a NovaSeq6000 SP flow cell (illumina) with paired-end 150bp reads. For Single Cell Sequencing: Library preparation was performed using the Tapestri platform (MissionBio) according to the manufacturers protocol (PN3354). Libraries were generated with a custom amplicon panel synthesized by MissionBio covering all exons of KRIT1, CCM2, PDCD10, and 7 amplicons covering somatic mutation hotspots in PIK3CA, per the COSMIC database. Up to three libraries were pooled and sequenced with a NextSeq Mid-Output 2x150bp kit (illumina). ddPCR for PIK3CA mutation validation was collected and analyzed using the Quantasoft software (v. 1.7.8.0917) SNaPshot data was collected using the ABI Foundation Data Collection software (v. 3.0)
Data analysis	For bulk sequencing: Sequencing data was processed according to the GATK (Broad Institute) best practices for somatic short variant discovery with slight modifications for “tumor-only” sequencing data. Variants were called using the Mutect2 function of GATK4 (v. 4.1.3.0) and annotated using snpEff (v. 4.3). As a secondary method for variant discovery we developed custom software designed specifically for the detection of somatic mutations in sequencing data from samples with no available normal tissue. This software was implemented as part of Gonomics, an ongoing effort to develop an open-source genomics platform in the Go programming language. Gonomics can be accessed at github.com/vertgenlab/gonomics. For Single Cell Sequencing:Data processing and QC was performed by the MissionBio cloud-based analysis pipeline (v. 1.10.0). Data quality for each nuclei barcode was determined using MissionBio recommended filtering settings. Data from low quality nuclei barcodes were removed prior to mutation analysis.

ddPCR for PIK3CA mutation validation was collected and analyzed using the Quantasoft software (v. 1.7.8.0917)
SNaPshot data was analyzed using the Genemapper software (v. 4.0)

For manuscripts utilizing custom algorithms or software that are central to the research but not yet described in published literature, software must be made available to editors and reviewers. We strongly encourage code deposition in a community repository (e.g. GitHub). See the Nature Research guidelines for submitting code & software for further information.

Data

Policy information about availability of data

All manuscripts must include a data availability statement. This statement should provide the following information, where applicable:

- Accession codes, unique identifiers, or web links for publicly available datasets
- A list of figures that have associated raw data
- A description of any restrictions on data availability

All data and reagents will be made available upon reasonable request. Transgenic mouse lines not available through public repositories are available from Mark Kahn under a material transfer agreement with the University of Pennsylvania. DNA sequencing data are available on request from Douglas Marchuk. The data are not publicly available due to them containing information that could compromise research participant privacy and consent. Public datasets used in this research are available at the following links: COSMIC (cancer.sanger.ac.uk/cosmic), dbSNP (ncbi.nlm.nih.gov/snp), 1000 Genomes Project (internationalgenome.org), ExAC (gnomad.broadinstitute.org)

Field-specific reporting

Please select the one below that is the best fit for your research. If you are not sure, read the appropriate sections before making your selection.

☒ Life sciences ☐ Behavioural & social sciences ☐ Ecological, evolutionary & environmental sciences

For a reference copy of the document with all sections, see nature.com/documents/nr-reporting-summary-flat.pdf

Life sciences study design

All studies must disclose on these points even when the disclosure is negative.

Sample size	For mouse experiments: Sample sizes were estimated based on our previous experience with the neonatal CCM model and microCT quantification of lesion volume, as previously described. For human experiments: Bulk sequencing analysis used all samples with available DNA obtained via biobank or clinical collaborators. snDNAseq samples used all samples for which multiple somatic mutations were identified, and sufficient tissue was available to perform analysis.
Data exclusions	For mouse experiments: All neonatal experimental and control animals were littermates and none were excluded from analysis at the time of harvest. Experimental animals were excluded at the pre-defined point: (i) failure to properly inject the inducing agent (4OHT, tamoxifen, rapamycin) and (ii) observation of significant leakage or neurologic symptoms. For human experiments: Several samples were excluded due to poor sequencing quality/depth, insufficient for the detection of somatic mutations and only where insufficient DNA was available for further sequencing.
Replication	For mouse experiments: Data were replicated over multiple litters and different breeding pairs of animals. For human experiments: Presence of somatic PIK3CA mutations were validated by ddPCR using available probesets (E542K, E545K, H1047R).
Randomization	For mouse experiments: Mice of the requisite genotype were randomly selected to receive the drug or vehicle.
Blinding	For neonatal mouse experiments: Pups were injected with 4OHT in a blinded fashion without knowledge of genotypes. For microCT quantification - Tissue processing, imaging, and volume quantification were performed in a blinded manner by investigators without any knowledge of genotype and experimental details. For bulk sequencing of human samples: All sequencing and variant calling of clinical samples was performed blinded to familial/sporadic status and any preexisting genetic data.

Reporting for specific materials, systems and methods

We require information from authors about some types of materials, experimental systems and methods used in many studies. Here, indicate whether each material, system or method listed is relevant to your study. If you are not sure if a list item applies to your research, read the appropriate section before selecting a response.

Materials & experimental systems

n/a	Involved in the study
☐	☒ Antibodies
☐	☒ Eukaryotic cell lines
☒	☐ Palaeontology and archaeology
☐	☒ Animals and other organisms
☐	☒ Human research participants
☒	☐ Clinical data
☒	☐ Dual use research of concern

Methods

n/a	Involved in the study
☒	☐ ChIP-seq
☐	☒ Flow cytometry
☒	☐ MRI-based neuroimaging

Antibodies

Antibodies used

For IHC: rat anti-PECAM1/CD31 (1:200; HistoBioTec, DIA-310), goat anti-KLF4 (1:100; R&D Systems, AF3158), goat anti-GFP (1:100; Rockland Immunochemicals, 600-101-215), rabbit anti-ERG (1:100; Abcam, ab110639) , rabbit anti-phospho-S6 (1:200, Cell Signaling Technologies, 4858S); Fluorescence-conjugated Alexa Fluor secondary antibodies were used (1:500, Invitrogen) according to the primary antibody species and counterstained with DAPI (1:1000). anti-CD31, Bio Rad (MCA2388) 1:200 (5 µg/ml) anti-rat IgG (Alexa Fluor 488), ThermoFisher (A-21208), 1:400 (5 µg/ml)

For immunoblotting: rabbit anti-GAPDH (1:2,000, Cell Signaling Technologies, 2118), rabbit anti-phospho-AKT Ser 473 (1:1000, Cell Signaling Technologies, 4060), rabbit anti-phospho-S6 Ser 235/236 (1:1000, Cell Signaling Technologies, 4858), mouse anti-total AKT (1:1000, Cell Signaling Technologies, 2920) and mouse anti-total S6 (1:1000, Cell Signaling Technologies, 2317). eNOS (Cell Signaling Technology, #9586, 1:1000), GFP (Cell Signaling Technology, #2555, 1:5000), KLF4 (Cell Signaling Technology, #4038, 1:1000), Phospho-S6 (Ser 235/236) Ribosomal protein (Cell Signaling Technology, #4857, 1:4000), Phospho-S6 (Ser 240/244) Ribosomal protein (Cell Signaling Technology, #2215, 1:4000), S6-Ribosomal protein (Cell Signaling Technology, #2217, 1:4000), Phospho-AKT (Ser 473) (Cell Signaling Technology, #4060, 1:2000), Phospho-AKT (Thr 308) (Cell Signaling Technology, #4056, 1:1000), AKT (pan) (Cell Signaling Technology, #4685, 1:2000), Tubulin (Cell Signaling Technology, #2148, 1:5000). Secondary antibodies are peroxidase-conjugated Goat IgGs (1:5000) purchased from Jackson Immuno Research Labs.

Validation

Validation of primary antibodies as determined by manufacturer. Secondary antibodies were validated for non-specific staining by no primary antibody negative controls.

Eukaryotic cell lines

Policy information about cell lines

Cell line source(s)

Pooled human umbilical vein endothelial cells (HUVECs) were purchased from Lonza (#CC- 5 2519)

Authentication

Describe the authentication procedures for each cell line used OR declare that none of the cell lines used were authenticated.

Mycoplasma contamination

HUVECs were tested negative for mycoplasma and cultured until the fourth passage.

Commonly misidentified lines
(See ICLAC register)

Name any commonly misidentified cell lines used in the study and provide a rationale for their use.

Animals and other organisms

Policy information about studies involving animals; ARRIVE guidelines recommended for reporting animal research

Laboratory animals

Cdh5-CreERT2, Slco1c1(BAC)-Cre, Slco1c1(BAC)-CreERT2, Pdgfb-CreERT2, Krit1flox, tetOn-KLF4, and Ptenflox animals have been previously described. R26-nTnG (JAX #023035), R26-LSL-Pik3caH1047R (JAX#016977) animals were obtained from the Jackson Laboratories. R26-CAGs-LSL-rtTA3 mice (JAX#029617) were generously provided by Lukas Dow. All experimental animals were maintained on a mixed-strain background and litter-mate controls were used for neonatal experiments unless otherwise indicated. Breeding pairs between 2 and 8 months of age were used to generate the animals of the indicated genotypes.

Wild animals

The study did not involve wild animals.

Field-collected samples

The study did not involve samples collected from the field.

Ethics oversight

All animals were housed in a pathogen-free environment in an AAALAC-approved vivarium at the University of Pennsylvania, and experiments were performed in accordance with the guidelines of the Institutional Animal Care and Use Committee (IACUC).

Note that full information on the approval of the study protocol must also be provided in the manuscript.

Human research participants

Policy information about studies involving human research participants

Population characteristics	Research participants comprise individuals from several sites including: University of Chicago, and the Barrow Neurological Institute. All individuals were diagnosed with a cerebral cavernous malformations, or a brain arteriovenous malformation.
Recruitment	Research participants include all who consented to the use of resected tissue for research purposes.
Ethics oversight	This study was approved by each institutions respective Institutional Review Board.

Note that full information on the approval of the study protocol must also be provided in the manuscript.

Flow Cytometry

Plots

Confirm that:

☒ The axis labels state the marker and fluorochrome used (e.g. CD4-FITC).

☒ The axis scales are clearly visible. Include numbers along axes only for bottom left plot of group (a 'group' is an analysis of identical markers).

☒ All plots are contour plots with outliers or pseudocolor plots.

☐ A numerical value for number of cells or percentage (with statistics) is provided.

Methodology

Sample preparation	Nuclei were isolated from human CCM/AVM tissue via dounce homogenization and filtered using a 30um mesh. Samples were stained with DAPI prior to sorting.
Instrument	BD FACSAria II
Software	FACSDiva v8.0.1
Cell population abundance	Nuclei typically constitute ~2% of total events in a CCM homogenate. Post-sort purity was determined for each sample via microscopy to ensure that nuclei aggregates comprised <5% of total nuclei (per manufacturer recommendations) prior to single-nucleus DNA sequencing.
Gating strategy	Initial selection of event populations was defined by positive signal in BV421-A corresponding to DAPI fluorescence. Further singlet discrimination was performed via FSC-H vs FSC-A as shown in Extended Data Figure 7b.

☒ Tick this box to confirm that a figure exemplifying the gating strategy is provided in the Supplementary Information.